Climate change effects on the marine characteristics of the Aegean and Ionian Seas

Christos Makris, Panagiota Galiatsatou, Konstantia Tolika, Christina Anagnostopoulou, Katerina Kombiadou, Panayotis Prinos, et al.

Ocean Dynamics
Theoretical, Computational and Observational Oceanography

ISSN 1616-7341
Volume 66
Number 12

Ocean Dynamics (2016) 66:1603-1635
DOI 10.1007/s10236-016-1008-1

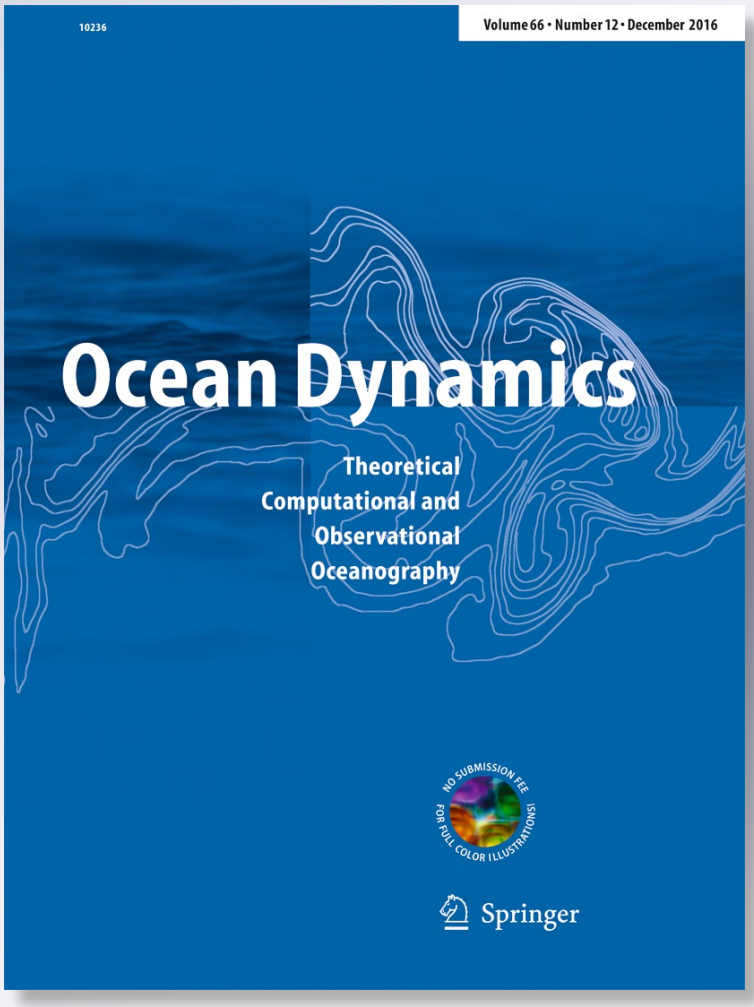

Springer

Ocean Dynamics (2016) 66:1603–1635
DOI 10.1007/s10236-016-1008-1

Climate change effects on the marine characteristics of the Aegean and Ionian Seas

Christos Makris[1] · Panagiota Galiatsatou[2] · Konstantia Tolika[3] · Christina Anagnostopoulou[3] · Katerina Kombiadou[1] · Panayotis Prinos[2] · Kondylia Velikou[3] · Zacharias Kapelonis[4] · Elina Tragou[5] · Yannis Androulidakis[1] · Gerasimos Athanassoulis[4] · Christos Vagenas[3] · Ioannis Tegoulias[3] · Vassilis Baltikas[1] · Yannis Krestenitis[1] · Theodoros Gerostathis[6] · Kostantinos Belibassakis[4] · Eugen Rusu[7]

Received: 15 February 2016 / Accepted: 4 October 2016 / Published online: 22 October 2016

Abstract This paper addresses the effects of estimated climate change on the sea-surface dynamics of the Aegean and Ionian Seas (AIS). The main aim is the identification of climate change impacts on the severity and frequency of extreme storm surges and waves in areas of the AIS prone to flooding. An attempt is made to define design levels for future research on coastal protection in Greece. Extreme value analysis is implemented through a nonstationary generalized extreme value distribution function, incorporating time harmonics in its parameters, by means of statistically defined criteria. A 50-year time span analysis is adopted and changes of means and extremes are determined. A Regional Climate Model (RegCM3) is implemented

Responsible Editor: Sandro Carniel

✉ Christos Makris
cmakris@civil.auth.gr

Panagiota Galiatsatou
pgaliats@civil.auth.gr

Konstantia Tolika
diatol@geo.auth.gr

Christina Anagnostopoulou
chanag@geo.auth.gr

Katerina Kombiadou
kobiadou@civil.auth.gr

Panayotis Prinos
prinosp@civil.auth.gr

Kondylia Velikou
kvelikou@geo.auth.gr

Zacharias Kapelonis
mail@zgk.gr

Elina Tragou
tragou@marine.aegean.gr

Yannis Androulidakis
iandroul@civil.auth.gr

Gerasimos Athanassoulis
mathan@central.ntua.gr

Christos Vagenas
christos.vagenas@met.fu-berlin.de

Ioannis Tegoulias
tegoulia@auth.gr

Vassilis Baltikas
vmpaltik@civil.auth.gr

Yannis Krestenitis
ynkrest@civil.auth.gr

Theodoros Gerostathis
tgero@teiath.gr

Kostantinos Belibassakis
kbel@fluid.mech.ntua.gr

Eugen Rusu
erusu@ugal.ro

[1] Laboratory of Maritime Engineering, Division of Hydraulics and Environmental Engineering, Department of Civil Engineering, Faculty of Engineering, Aristotle University of Thessaloniki, GR-54124 Thessaloniki, Greece

[2] Laboratory of Hydraulics, Division of Hydraulics and Environmental Engineering, Department of Civil Engineering, Faculty of Engineering, Aristotle University of Thessaloniki, GR-54124 Thessaloniki, Greece

[3] Department of Meteorology and Climatology, School of Geology, Faculty of Sciences, Aristotle University of Thessaloniki, GR-54124 Thessaloniki, Greece

with dynamical downscaling, forced by ECHAM5 fields under 20C3M historical data for the twentieth century and the SRES-A1B scenario for the twenty-first century. Storm surge and wave models (GreCSSM and SWAN, respectively) are used for marine climate simulations. Comparisons of model results with reanalysis and field data of atmospheric and hydrodynamic characteristics, respectively, are in good agreement. Our findings indicate that the dynamically downscaled RegCM3 simulation adequately reproduces the present general circulation patterns over the Mediterranean and Greece. Future changes in sea level pressure and mean wind fields are estimated to be small, yet significant for marine extremes. In general, we estimate a projected intensification of severe wave and storm surge events during the first half of the twenty-first century and a subsequent storminess attenuation leading to the resettlement of milder extreme marine events with increased prediction uncertainty in the second half of the twenty-first century.

Keywords Aegean and Ionian Seas · Climate change · Storm surges · Waves · Extreme value analysis · SRES-A1B

Abbreviations

AICc	Akaike Information Criterion correction
AIS	Aegean and Ionian Seas
AVISO	Archiving, Validation and Interpretation of Satellite Oceanographic data
BACC	BALTEX Assessment of Climate Change for the Baltic Sea basin
CCI	Climate Change Index (symbol: CCI)
CDF	Cumulative distribution function
EI	Error Index (symbol: EI)
EVT	Extreme Value Theory
GCM	Global Climate Model
GEV	Generalized extreme value
GEBCO	General Bathymetric Chart of the Ocean
GRACE	Gravity Research And Climate Experiment (NASA)
GreCSSM	Greek Climatic Storm Surge Model
HNHS	Hellenic Navy Hydrographic Service
HRP	Hit rate of percentiles (symbol: *HRP*)
IFS	Integrated Forecast System
IPCC	Intergovernmental Panel on Climate change
MAE	Mean absolute error
MeCSSM	Mediterranean Climatic Storm Surge Model
MLEs	Maximum likelihood estimates (symbol: *MLEs*)
MSL	Mean sea level (symbol: *MSL*)
NAO	North Atlantic Oscillation
POT	Peaks over threshold
RCM	Regional Climatic Model
RegCM3	Regional Climate Model 3rd version
SLH	Sea level height (due to storm surges) (symbol: *SLH*)
SLP	Sea level pressure (in the atmosphere) (symbol: *SLP*)
SLR	Sea level rise (long-term) (symbol: *SLR*)
SRES	Special Report on Emission Scenarios
SSI	Storm Surge Index (symbol: *SSI*)
SWAN	Simulating WAves Nearshore
SWH	Significant wave height (symbol: H_s)
WAM	WAve prediction Model

1 Introduction

Climate change is expected to affect the frequency, trajectory and intensity of storms (IPCC 2007, 2012) in many areas around the world. This projection has led to estimations of local increase of extreme water levels in the future, especially if the combined effect of rising sea level and high storm surges is taken into account (Wang et al. 2008). Furthermore, climate change may affect hydrodynamic conditions in nearshore areas driving consequent changes in the wave climate that may increase the vulnerability of coastal zones and their defences.

Several researchers have studied the effects of climate change on the wind, wave and storm surge characteristics around the world. Specific evidence of climate change impacts on atmospheric circulation patterns over Europe and the marine hydrodynamics of the European seas have been provided in a number of studies. Esteves et al. (2011) investigated the general metocean trends at the eastern Irish Sea. Grabemann and Weisse (2008) analysed present mean and extreme wave conditions in the North Sea and their possible future changes due to anthropogenic climate change. Van den Eynde et al. (2012) investigated the evolution of extreme winds, wave heights and storm surge levels in the Belgian part of the North Sea to assess the changes in the marine storminess. De Winter et al. (2012) studied the changes of the mean wave climate and the annual maxima of wave heights with return periods of up to 10^4 years

[4] Section of Ship and Marine Hydrodynamics, School of Naval Architecture and Marine Engineering, National Technical University of Athens, 9, Heroon Polytechniou str., Zographos, Athens GR-15773, Greece

[5] Department of Marine Sciences, University of the Aegean, University Hill, GR-81100 Mytilene, Lesvos Island, Greece

[6] Department of Naval Architecture, Faculty of Technological Applications, Technological Institute of Athens, Aegaleo, Athens GR-12210, Greece

[7] Department of Applied Mechanics, Dunarea de Jos Galati University, 9 Traian St., Bl. W3 Ap. 11, Galati 6200, Romania

in front of the Dutch coast under the SRES-A1B scenario. The basic features of the wave climate and its changes in the south-western Baltic Sea were presented by Soomere et al. (2012). An assessment of overall climate change impacts on the Baltic Sea was reported by The BACC Author Team (2008).

Several studies focus either on the entire basin or on parts of the Mediterranean Sea, such as the eastern Spanish coastal zone, the Adriatic, the Aegean, the Ionian, the Levantine and the Libyan Seas. Lionello et al. (2008) studied the Mediterranean wave climate, based on 30-year-long (2071–2100) simulations of the wind-wave fields with the WAve prediction Model (WAM) under the SRES-A2 and B2 scenarios. They also simulated the wind-wave fields for a near-past reference period of equal duration (1961–1990), in order to represent the present climate. Results showed that changes of significant wave height (SWH), wind speed and atmospheric circulation were consistent and that marine storms will probably be milder in the future than in the present climate. Benetazzo et al. (2012) analysed the wave climate of the Adriatic Sea, under the SRES-A1B scenario for the 2070–2099 period, and also concluded that a milder future wave climate is expected, even though wave severity may intensify locally. Future regional climate projections at a rather high spatiotemporal resolution for the projected wave fields of the northwestern Mediterranean Sea were obtained by Casas-Prat and Sierra (2013). Relative changes of SWH reached up to ±10 % for the mean climate and up to ±20 % for extremes. Androulidakis et al. (2015) estimated a decreasing trend in storminess under the SRES-A1B scenario, mostly related to the frequency, duration and spatial coverage of local storm surge maxima and in the Mediterranean. Relevant climate change studies on sea-surface dynamics specifically targeted on the east-central Mediterranean Sea and particularly on the Aegean and Ionian Seas (AIS) have not been previously reported. Hence, in order to address the aforementioned information gap, the main aims of the present paper are the following:

(i) To estimate the future climate over the AIS, with a special focus on the simulation of wind and sea level pressure (*SLP*) fields for the twenty-first century
(ii) To assess the effects of climate change on the sea-surface dynamics of the AIS, i.e. estimate changes in waves and storm surges up to 2100
(iii) To quantify the severity and frequency of extreme wave and storm surge events in the AIS in order to produce design levels for coastal protection works in Greece (next step of the research project referenced in the Acknowledgments)
(iv) To identify specific mechanisms of regional climate change in the AIS, i.e. estimate the projected overall attenuation or amplification of storminess in the AIS towards the end of the twenty-first century

Therefore, an attempt is made to investigate the effects of potential climate change on the atmospheric features (wind and pressure fields), the wave characteristics and the storm surges in the AIS. The Regional Climate Model (RCM), RegCM3 (Giorgi et al. 1993a, 1993b), is used; it is forced by the Global Climate Model (GCM) of the Max Planck Institute for Meteorology ECHAM5 (Roeckner et al. 2003) simulated fields, produced under 20C3M historical scenario for the twentieth century and the SRES-A1B scenario for the twenty-first century.

The specific goals of our analysis are designated as follows. The simulated wind and *SLP* fields (temperature and precipitation are not presented herein) are compared and evaluated against available reanalysis data (Section 3.1) for the time span 1981–2000. New data archives for wind and *SLP* fields are produced for the entire Mediterranean basin covering the period up to 2100 (Tolika et al. 2015). The RegCM3 climate simulations are implemented with a downscaled spatial resolution in the AIS domain, one-way nested to the coarser Mediterranean domain. We attempt to evaluate the dynamically downscaled atmospheric fields against reanalysis data for the twentieth century.

The Simulating WAves Nearshore (SWAN) model (Booij et al. 1999, Ris et al. 1999) is used for the simulations of the past, current and future wave climate. A two-dimensional barotropic model of hydrodynamic ocean circulation (Greek Climatic Storm Surge Model; GreCSSM) is used to simulate the past, current and future storm surge climate. GreCSSM is based on the numerical model simulating the storm-induced sea-surface variations, which was developed by De Vries et al. (1995), validated and implemented by Krestenitis et al. (2011). GreCSSM is one-way nested to the coarser implementation of the same model for the entire Mediterranean region (Mediterranean Climatic Storm Surge Model; MeCSSM), presented by Androulidakis et al. (2015). Both the wave and storm surge models were calibrated with available model, satellite and field data (Sections 3.2 and 3.3).

To assess the climate change effects on the wave and storm surge characteristics of the AIS, the changes of 50-year patterns for the mean and extreme waves and storm surges are determined until the end of the twenty-first century. We adopted a 50-year time span analysis (1951–2000, 2001–2050 and 2051–2100) to increase the reliability of extreme value analysis of marine characteristics.

To quantify climate change effects on the severity and frequency of extreme marine events, extreme value analysis of waves and storm surges is applied. Comparisons of certain hydrodynamic characteristics are presented for the three 50-year periods indicating estimated changes between the past, current and future extreme marine climate of the AIS. Moreover, we estimate the prediction uncertainty, future trends and return levels of the simulated hydrodynamic features, i.e. characteristics of wave heights and storm surges. The results can be used to estimate coastal vulnerability indexes and to produce design levels for future coastal protection works in the AIS. The mean sea level (*MSL*) and sea level rise (*SLR*) projections in the Mediterranean and the AIS are also concisely reviewed based on available state-of-the-art data in the relevant literature.

Subsequently, the study area and its main atmospheric (winds, pressures and storms) patterns and marine (*MSL*, waves and storm surges) characteristics are presented in Section 2. The implemented models are presented in Section 3, emphasizing on their main characteristics, spatio-temporal resolutions and validation attributes. In Section 4, the past, current and future patterns of winds, *SLP*, waves and storm surges are analysed for mean and extreme values, and the climate change signals are identified, followed by discussion and comparisons against existing literature. The main conclusions are presented in Section 5.

2 Study area

The study area (Figs. 1b and 2b) is located in the east-central part of the Mediterranean Sea, between longitudes 19.4° E and 30° E and latitudes 30° N and 42° N. It mostly concerns the aquatic bodies that abut the Greek mainland and the western coasts of Anatolia (Turkey), comprising the AIS (Fig. 2b, c: Ionian, North and South Aegean Seas). The overall simulation domain also covers part of the south-central Mediterranean, the Libyan Sea and a small westernmost part of the Levantine Sea (Fig. 2c). The complicated continental orography and the presence of a very large number of islands, mostly in the Aegean archipelago, render the study area very interesting from a climate modelling viewpoint. Furthermore, the respective water bodies have a rapidly varying bathymetry with deep basins and extensive, rather shallow, continental shelves and extremely complex coastlines. The latter are divided almost equally into steep reflective rocky formations, frequently interrupted by mostly short (and rarely wide) dissipative beaches ideal for touristic activities. Moreover, both Greek and Turkish coastal zones are highly populated with numerous coastal cities, ports, harbours and marinas, river deltas, protected wetlands, islets, insular formations, highly irregular coastlines and lowland elevation coastal areas. These

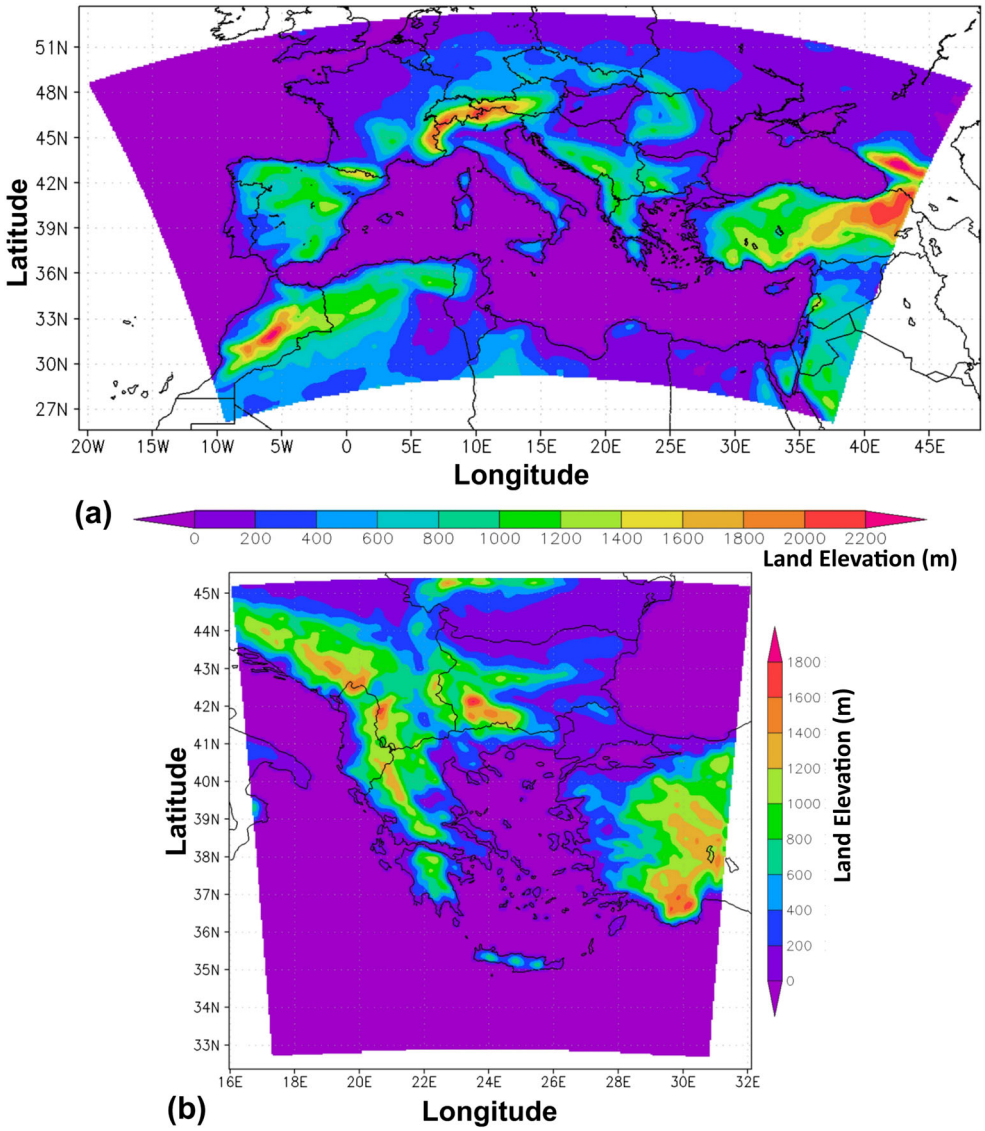

Fig. 1 Topography and land maps of the study area: **a** level I (25 km domain) land elevation (m) for RegCM3-25Km simulations; **b** level II (10 km domain) land elevation (m) for dynamically downscaled RegCM3-10Km simulations

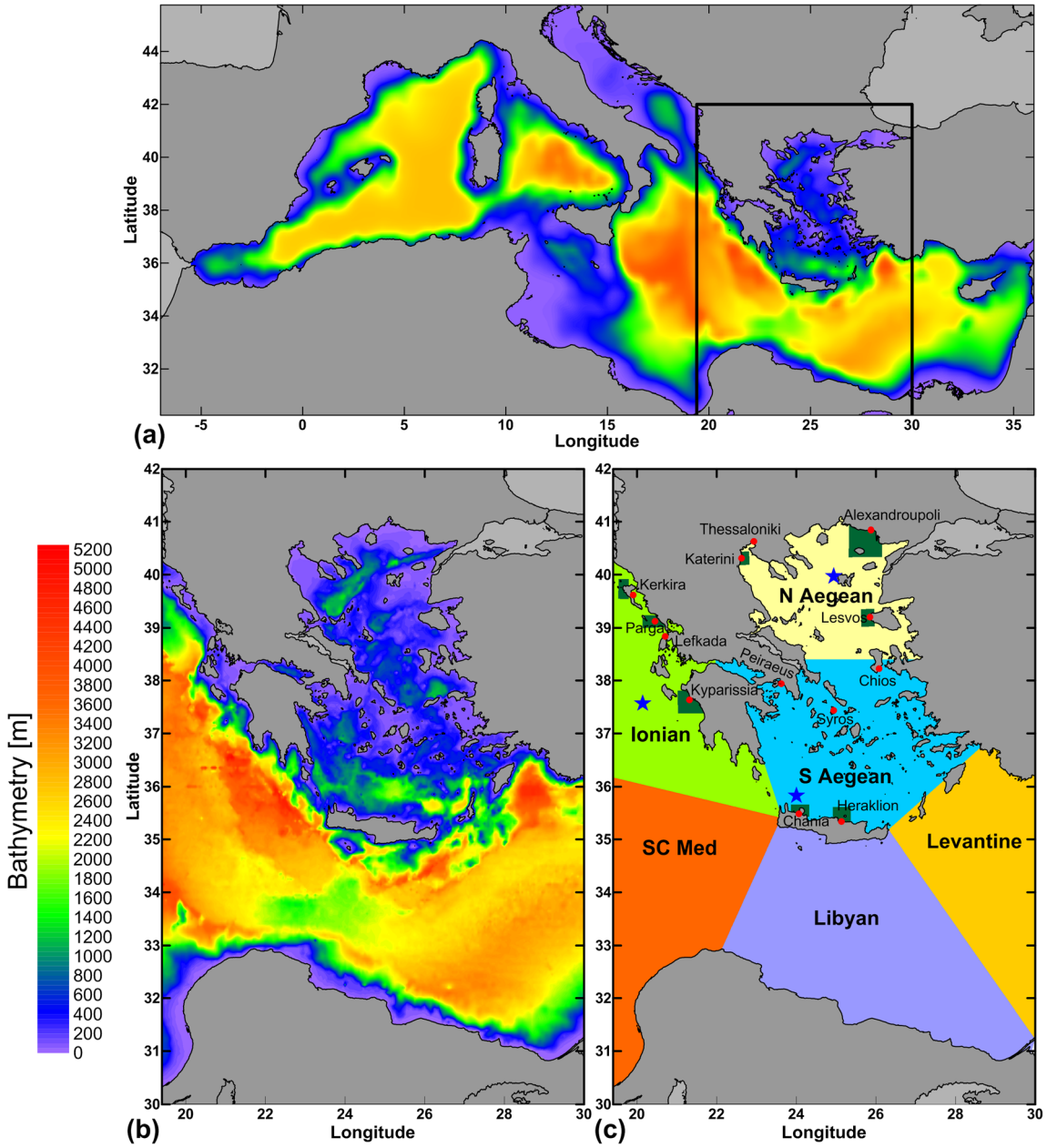

Fig. 2 Marine maps of the study area: **a** level I bathymetry (m) for marine simulations (1/5° to 1/10° resolution); **b** level II bathymetry (m) for marine simulations (1/20° resolution); **c** 6 subregions of interest (N. and S. Aegean, Ionian, SC Med, Libyan and Levantine) denoted by *different colours*, 8 marine areas (Kerkira, Parga, Kyparissia, Chania, Heraklion, Lesvos, Katerini, Alexandroupoli) where extreme value analysis is conducted denoted by *green hatches*, 13 coastal gauges denoted by *red dots* and 3 offshore stations denoted by *blue stars*

low coastal plains are at high inundation risk in cases of extreme storm surge events, especially when combined with high wave-induced set-up in the surf zone and run-up on beaches and waterfronts. The particular coastal topography of certain marine areas (Fig. 2c) makes them potentially prone to coastal flooding even for moderate sea level elevations due to storm surges. Overall, the topographic complexity of the entire Greek and the western Turkish coastlines plays an important part in the configuration of the wind regime, the wave field and the storm-induced sea level variations.

2.1 Atmospheric circulation and wind patterns

The atmospheric circulation over the Mediterranean basin is strongly affected by the main atmospheric centres of action: the permanent ones, i.e. the Azores high and the Icelandic low over the North Atlantic Ocean and the seasonal semi-permanent ones, i.e. the winter Siberian high-pressure system, the summer Asian thermal low, the West African heat low and the high-pressure systems of Europe and Balkan Peninsula (Barry and Carleton 2001). Cold air masses are observed in Asia and Eastern

Europe due to the Siberian high, which is replaced by a centre of low pressure during the warm period (viz. spring and summer seasons), developed above South Asia and Middle East (known as Asian thermal low). This low-pressure system and the Balkan Peninsula high pressure are the two centres of action that result in the Etesian winds over the Aegean Sea during the warm period (Anagnostopoulou et al. 2014).

However, the Mediterranean basin is also a major source of origination or reinforcement of cyclones (Gil et al. 2002). In its western part, there are three main regions of cyclogenesis (Trigo et al. 1999): (a) the Genoa centre; (b) the Saharan cyclones, dominant during spring; and (c) the Iberian peninsula thermal lows with three discrete centres (viz. eastern, western and central), forming from late spring through the summer, particularly pronounced between June and August. In the east-central and eastern Mediterranean, four regions of cyclogenesis are distinguished (Trigo et al. 1999, Maheras et al. 2001): (a) the Aegean Sea, one of the major cyclogenesis regions during winter and spring; (b) the eastern Black Sea, which contains an all-year major centre that is more pronounced during July and August; (c) the vicinity of Cyprus, which is also a year-round cyclone source; and (d) the Middle East with main centres over Syria and Iraq. The latter are the main regions of summer cyclogenesis in the eastern Mediterranean due to the extension of the Indian monsoon low.

The prevailing atmospheric circulation patterns in the AIS are mainly characterized by northerly winds. Specifically during the cold period (viz. autumn and winter seasons), northeasterly winds prevail in the northern Aegean Sea and northerly winds in its central and southern parts. Winds are mainly of a western component in the Ionian Sea. The strongest winds, related to regions of large wave heights in the Aegean Sea, are mainly observed in its northern and central offshore parts, as well as in the southwestern Aegean boundary, i.e. the straits between Peloponnesus and Crete (Vagenas et al. 2014). During the warm period, the Aegean Sea is predominated by the Etesians (or Meltemia), which constitute one of the most persistent localized wind systems in the world (Anagnostopoulou et al. 2014). The Etesians are dominant mainly during summer and early autumn over the Aegean Sea and parts of the eastern Mediterranean; Etesians are northeasterlies in the northern Aegean Sea, turn to northerlies in the central and southern Aegean Sea and to northwesterlies near the southwestern coasts of Turkey (Savvidis et al. 2004).

2.2 Wave characteristics

The wave climate of the AIS is strongly affected by physical mechanisms taking place in the Mediterranean Sea. Due to very limited flow exchange with the Atlantic Ocean through the Strait of Gibraltar, the Mediterranean is an effectively closed basin regarding wave phenomena. Thus, the dominant wave patterns are mainly dependent on the wind conditions, the varying Mediterranean bathymetry and the interaction with complex coastlines and numerous islands. The Mediterranean basin can be practically viewed as comprising two distinct parts connected via the Strait of Sicily.

Focusing on the main study area of the AIS, the Ionian is a marginal sea with a semi-open basin containing a relatively small number of islands in proximity to the mainland. Winter mean values of the SWH, H_s, for recent decades vary from 1.2 to about 1.7 m from the northern to the southern Ionian Sea (Athanassoulis and Skarsoulis 1992, Athanassoulis et al. 2004, Soukissian et al. 2008). The most frequent mean wave directions are from the west-southwest sector due to Libeccio wind and from the southeast sector due to Sirocco (Zecchetto and De Biasio 2007). The Bora winds from the northeast sector (Dykes et al. 2009) have no significant effect on the wave field due to the strong sheltering offered by the mainland, especially the Pindus mountain range. A more diverse wave regime is found in the Aegean Sea due to its complex bottom topography, the presence of channels combined with fetch regions of moderate extent and the numerous islands. Being cut out from the rest of the Mediterranean by the island of Crete and other islands of the outer Hellenic Arc, the Aegean Sea exhibits lower H_s values. Winter mean values for recent decades span from about 0.6 to 1.3 m with maxima located at the northeastern Aegean, the central Aegean (north of Cyclades island group), the Crete-Kythira and Crete-Karpathos straits (Athanassoulis et al. 2004, Soukissian et al. 2008). The directionality of waves in the Aegean during summer is dominantly of the north sector due to the Etesians, which diminish during the winter when violent cyclonic storms occur (Soukissian 2005). These winter storms produce almost exclusively north and south sector seas, while western and eastern events appear with much lower frequency (Christopoulos 1997).

2.3 Storm surge characteristics

The storm surges in the AIS are mainly induced by the inverse barometer effect and only locally by strong winds, caused by usually enfeebled extra-tropical storms that follow a west-to-east path over the Mediterranean Sea (Krestenitis et al. 2011). Sea level extremes are mainly related to storm surges rather than to the combination of tides and surges in the study area (Marcos et al. 2009).

Tsimplis and Vlahakis (1994) investigated the effect of atmospheric pressure and surface winds on the sea level variability of the Aegean Sea. They found a very high spatial correlation between sea level height (*SLH*) and *SLP*, as well as meridional (North-to-South) wind components, explaining

90 % of total *SLH* variations throughout the central and eastern parts of the study area. Tsimplis and Blackman (1997) analysed extreme sea levels from 18 ports in the AIS using *SLH* recordings from 1982 to 1989. They found higher 50-year return levels (by 0.2 to 0.3 m) in stations located in the North Aegean than those of the central and southern AIS, in which the predicted return levels were of similar magnitudes. They calculated 50-year return levels that ranged between 0.35 and 0.37 m in the South and Central Aegean (Chania, Peiraeus, Chios and Syros) and between 0.64 and 0.70 m in the North Aegean (Thessaloniki and Alexandroupoli). By assuming higher return levels (100 to 500 years) the related increase in *SLH* was low (of the order of 5 cm).

Marcos et al. (2011) extensively studied the changes in storm surge characteristics over the Mediterranean Sea using different climate projections. Their results showed that an average of 4 to 5 moderate surge events (>0.15 m) per year occurred in the AIS in the past, with the highest frequencies in the North Aegean. However, they found that these frequencies are expected to decrease by 1 to 2 events per year under the SRES-A1B scenario towards the end of the twenty-first century. The related changes of 50-year return levels of positive surges during 2090–2099 with respect to the ones of 1990–1999 were of the order of −3 to −4 cm in the AIS, apart from the Sea of Crete (south-most part of the South Aegean) and the Libyan Sea, where the reduction was lower (−2 cm). Similarly, Jordà et al. (2012) estimated decreasing trends of −0.18 ± 0.04 mm/year for *SLH* in the eastern Mediterranean under SRES-A1B scenario. They estimated an increase of the storm surge seasonal cycle, i.e. a decrease of winter-autumn occurrence frequencies accompanied by an increase of spring-summer ones.

Conte and Lionello (2013) examined surges in the Mediterranean Sea under SRES-A1B scenario using various climatic datasets for the 1951–2050 period. Their results showed ±5 % future changes for positive surges in the area, whereas a weighted ensemble mean of all climate simulations showed a robust and widespread reduction of surge magnitudes. They also found that the contribution of *SLP* and wind on positive surges in the AIS is of the order of 55–75 % and 25–45 %, respectively. This was corroborated by Androulidakis et al. (2015), who found similar behaviour with slightly higher contribution of *SLP* (65–75 %) to storm surge maxima in the AIS.

2.4 Mean sea level

Projections of sea level changes due to short time-scale processes, such as waves and storm surges, should be superimposed to projections of long-term *MSL*, mainly depending on changes in the hydrographic characteristics (i.e. volume changes) and the net water mass addition due to ice melting. Although in a few previous studies the *MSL* variability in the Mediterranean during the twenty-first century was investigated, most of them include only on the steric or thermosteric effect.

Marcos and Tsimplis (2008) first pointed out the complexity of the problem using various GCM projections under three scenarios (i.e. committed climate change, SRES-A1B and A2). They showed lack of agreement on sea level trends between the models, due to coarse resolution and inadequate connection with the Atlantic, and therefore stressed the need for high-resolution RCM projections. Tsimplis et al. (2008) analysed the results of a high resolution, air-sea coupled climate model under the SRES-A2 scenario, projecting a Mediterranean maximum steric *SLR* of 25 cm for the end of the twenty-first century. For the AIS region, the steric *SLR* was even smaller, viz. less than 15 cm in the Ionian and less than 5 cm in the Aegean Seas. The calculated differences relied on analysis of 30-year time intervals, namely between 2070 and 2099 and 1961–1990, yet implied that a globally pessimistic scenario may not result in high sea levels for the AIS.

Carillo et al. (2012) examined the role of steric effect on the future *MSL* change extending their analysis until 2050. They projected a thermosteric *SLR* of about 5 cm for the AIS by 2050 (vs. 1951–2000) under the SRES-A1B scenario, which could become slightly higher (12 cm for the Ionian and 7 cm for the Aegean) under different boundary conditions connecting the Mediterranean with the Atlantic. More recently, Adloff et al. (2015) investigated the response of the Mediterranean to six different climate change scenarios (SRES-A1B, B1 and A2 under different forcings), and found larger basin-averaged thermosteric *SLR* of about 10 cm and 30–40 cm for the 2000–2050 and 2050–2099 periods, respectively. To assess total *SLR*, other components should be included (e.g. mass addition due to land ice melting), adding between 15 and 30 cm to the thermosteric component, according to the IPCC AR5 (IPCC 2013). This value agrees well with recent estimates of *MSL* trend due to changes in the mass (GRACE program), corresponding to about 2.5 mm/year, averaged over the whole Mediterranean for the period from January 2003 to July 2013 (Tsimplis et al. 2013). If this trend remains constant, the mass addition should raise the Mediterranean *MSL* by approximately 12 cm by 2050 and 25 cm by 2100. Both Carillo et al. (2012) and Adloff et al. (2015) draw attention to the large uncertainty introduced by the hydrographic characteristics of the Atlantic prescribed as boundary conditions to the Mediterranean model; Adloff et al. (2015) conclude that the choice of the near-Atlantic surface water evolution has the largest impact on the thermosteric sea level ranges, larger than the choice of the socio-economic scenario. This conclusion should also apply to a more regional scale, regarding the role of the Black Sea hydrographic characteristics to the evolution of the Aegean *MSL*, as it is an area susceptible to buoyancy changes imported from the Dardanelles (Zervakis et al. 2000). The only regional multimodel assessment of future sea level change of the whole Mediterranean basin has been carried out in the

framework of the CIRCE project (Gualdi et al. 2013), showing a positive steric trend of 0.29 ± 0.13 cm/year, or a total steric rise between 7 and 12 cm for the 2021–2050 period (vs. 1961–1990) under the SRES-A1B scenario.

In general, compared to the significant scientific progress at global scale, the advances at the Mediterranean scale remain small in terms of *MSL* assessment from regional ocean models (Slangen et al. 2016), especially due to uncertainties regarding exchanges with neighbouring seas.

3 Methods and models for the analysis of the marine climate

The numerical models, used for the climate simulations of the weather conditions and the marine characteristics of the AIS, are presented together with the statistical methods for correcting bias and deriving extreme values. The main attributes of an RCM, a wave and a storm surge model are briefly described (Table 1) together with validation results for assessing their performance.

A 50-year time span analysis is adopted, in order to meet two basic requirements: (a) the annual maxima within each period should be considered adequately stationary and (b) the dataset of each period should be large enough to provide a good fit of the marginal extreme value distributions. The simulations cover the 150-year period 1950–2100 (Table 1). Results are derived for a reference period (1951–2000), a current period (2001–2050; representative of the present and near future climate) and a future period (2051–2100). For the reference period the RCM is forced by GCM fields which are

Table 1 Basic parameterizations, major attributes and simulation scheme properties of the climate (RegCM3), wave (SWAN) and storm surge (MeCSSM/GreCSSM) models. Differences between the coarse (level I) and downscaled (level II) implementations for all the models

Attribute/parameterization	Coarse implementation	Downscaled implementation
Computational domain	level I	level II
Bathymetry	GEBCO (Becker et al. 2009)	
Climate model	RegCM3-25Km	RegCM3-10Km
Location	Mediterranean basin	East-central Mediterranean region (incl. Aegean and Ionian Seas)
Driving field	ECHAM5	Nested to RegCM3-25Km
Forcing	Control run (1951–2000) under 20C3M	
	Scenario-based run (2001–2100) under SRES-A1B	
Number of grid points	192 × 108	128 × 144
Number of vertical levels	18	18
Spatial resolution	25 km	10 km
Simulation time span	January 1, 1950–December 31, 2100	
Integration time step	60 s	30 s
Terrain and land use resolution	10 min	3 min
Cumulus scheme	Grell (1993)	MIT – Emanuel (1991)
Convective closure scheme	Fritsch and Chappell (1980)	
Planetary boundary layer scheme	Holtslag et al. (1990)	
Wave model	SWAN	
Spatial resolution	1/5° × 1/5°	1/20° × 1/20°
Directional step	10°	
Frequency range	0.04–1 Hz	0.056–1 Hz
Integration time step	10 min	
Integration scheme	BSBT	
Boundary input	–	Nested to SWAN level I simulation
Storm surge model	MeCSSM	GreCSSM
Spatial resolution	1/10° × 1/10°	1/20° × 1/20°
Integration time step	60 s	30 s
Air/sea interface friction	Smith and Banke (1975)	
Bottom friction approach	Wang (2002)	
Boundary input	–	Nested to MeCSSM
Boundary/nesting technique	Dirichlet/open sea boundary with estimated free surface	
Eddy viscosity treatment	Boussinesq hypothesis: Smagorinsky model for horizontal eddies	

produced under the historical 20C3M scenario that incorporates an increase of greenhouse gasses as observed through the twentieth century (IPCC 2001). For the twenty-first century projections, the RCM is forced by GCM fields simulated under the SRES-A1B emission scenario. The latter is based on the assessment that all the energy sources will be equally used, and is characterized as an intermediate scenario with the CO_2 concentrations reaching up to 700 ppm until the end of twenty-first century (IPCC 2001). SRES-A1B belongs to scenarios that describe a future world of very rapid economic growth with prompt introduction of new and more efficient technologies and fast increase of global population that peaks in the midst of the twenty-first century, but declines thereafter.

Two simulation levels are used for all models: level I includes the entire Mediterranean Sea with a model-dependent spatial resolution (Figs. 1a and 2a) and level II covers an east-central Mediterranean subsection including the AIS (Figs. 1b and 2b). The computational domains of Fig. 1 refer to the atmospheric simulations and of Fig. 2 to the hydrodynamic simulations. In addition, level II is divided into discrete subregions (e.g. South/North Aegean, Ionian, etc. denoted by different colours in Fig. 2c) and the extreme value analysis focuses on eight nearshore areas of interest (denoted by green hatches in Fig. 2c) due to potentially high vulnerability to flooding.

3.1 The Regional Climate Model

RegCM3 (Giorgi et al. 1993a, 1993b) is used in its modified and improved form (Giorgi and Mearns 1999, Pal et al. 2007) to incorporate the complex terrains and sharp orography of the study domains. The dynamical component of RegCM3 is a compressible, finite difference model with hydrostatic balance and vertical σ-coordinates using a split-explicit time-integration scheme along with an algorithm for reducing horizontal diffusion in the presence of steep topographical gradients. Two different implementations were performed, namely RegCM3-25Km (level I) and RegCM3-10Km (level II), with the finer one nested into the coarser one. The basic parameterizations (spatial resolutions, convective precipitation schemes and closure assumptions) for both simulations are shown in Table 1.

The dynamically downscaled simulation with RegCM3 at higher resolution has been proven to provide better results of climatic parameters than the one performed at lower resolution over Greece and the AIS (Tolika et al. 2015). Moreover, a new evaluation of results is presented concerning modelled fields of both wind (Fig. 3) and mean *SLP* (Fig. 4) in comparison to the ERA-Interim data (Berrisford et al. 2011, Dee et al. 2011). The latter are available from January 1979 up to present time, derived from the IFS 2006 edition (Cy31r2). They include four-dimensional variational analysis at a spatial resolution of 80 km

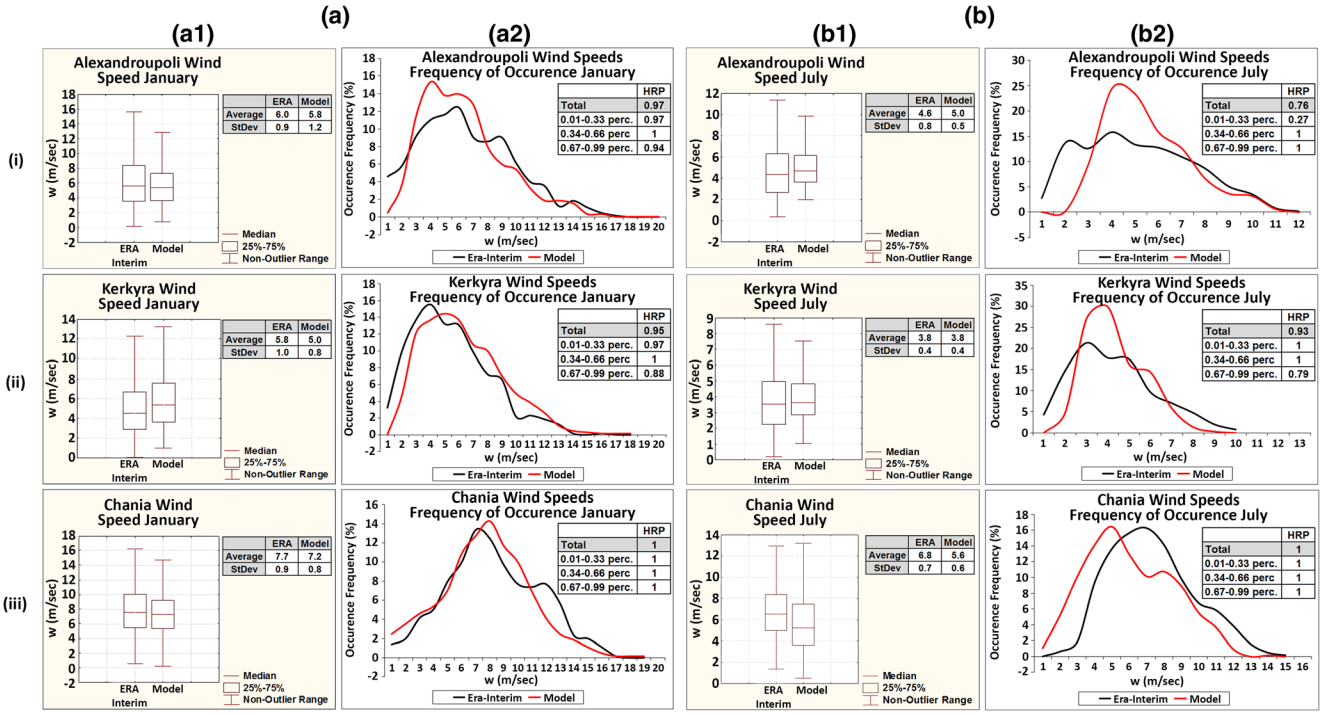

Fig. 3 Evaluation of RegCM3 model results (winds) for three locations *(i)* Alexandroupoli, *(ii)* Kerkyra and *(iii)* Chania over the domain of study for **a** January (*left-panel graphs*) and **b** July (*right-panel graphs*) in comparison with the ERA-Interim data for the period 1981–2000. Graphs of the first and third columns (*a1* and *b1*) are box-plots of wind speeds (m/s), and graphs of the second and fourth columns (*a2* and *b2*) are occurrence frequency (%) distribution diagrams. Text boxes of the box plots (*a1* and *b1*) refer to the average and standard deviation values of modelled and ERA-Interim wind speeds (m/s); text boxes of the distribution graphs (*a2* and *b2*) refer to the respective HRP index

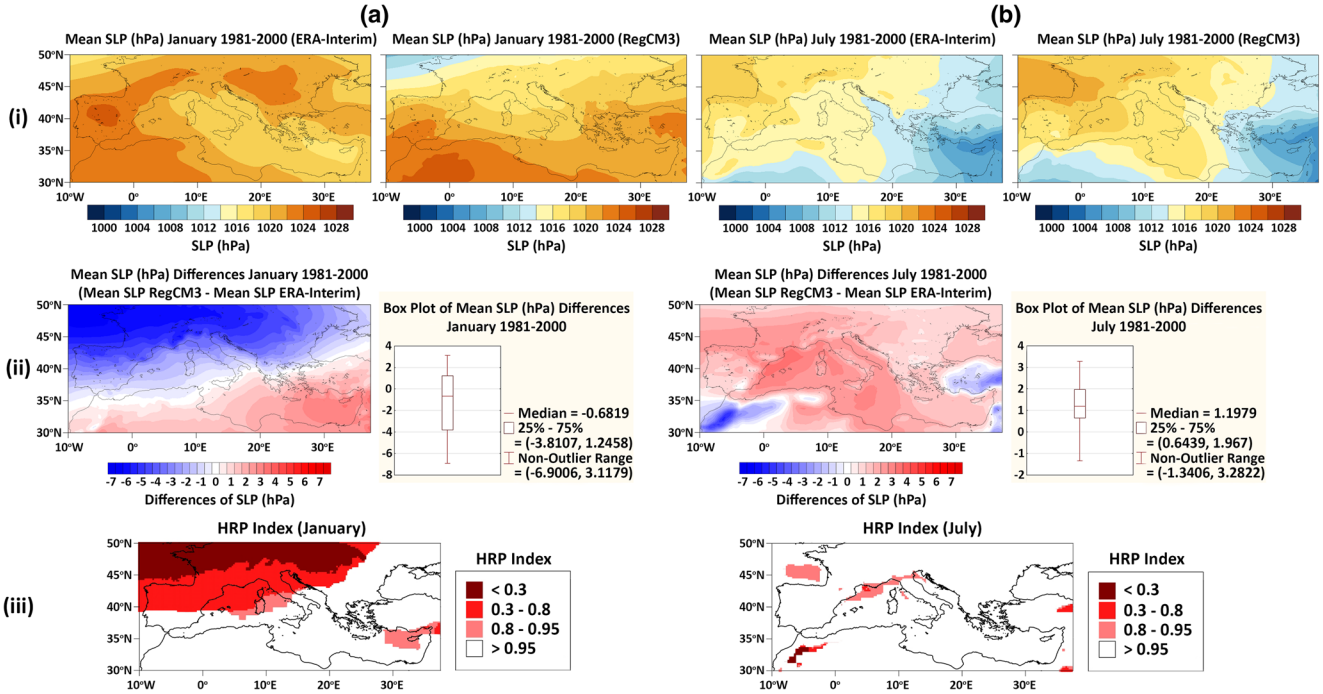

Fig. 4 *(i)* Monthly *SLP* (hPa) spatial distribution from ERA-Interim and RegCM3 for **a** January and **b** July (*upper row of graphs*). *(ii)* Spatial distribution maps of mean *SLP* differences (%) between ERA-Interim and RegCM3 fields and box plots of the mean *SLP* differences (*mid row of graphs*). *(iii)* Spatial distribution maps of the *HRP* index for **a** January and **b** July (*lower row of graphs*); the regions that are not coloured are the ones where *HRP* index has values greater than the limit of 0.95, which indicates no imperative need for bias correction in climate data for the purposes of the present paper

and 60 vertical levels from surface up to 0.1 hPa. The relevant fields were downscaled to a finer spatial resolution of 0.125° × 0.125° (i.e. spatial discretization step around 12.5 km in the AIS), in order to closely resemble the RegCM3-10Km resolution. In the present study, we used both wind and *SLP* data for the period 1981–2000. Specifically, three characteristic regions were selected for the validation of the wind fields: (a) Alexandroupoli in northern Greece; (b) Kerkira in the island of Corfu (northern Ionian Sea); and (c) Chania in the island of Crete (southern Aegean Sea). Representative grid points were selected for these areas, *sc.* one from the RegCM3-10Km simulation archive and the nearest one from the ERA-Interim data archive; these were closer to each other than available meteorological stations in the area. Statistical measures were calculated to define the simulation skill of the model used.

Figure 3 illustrates the RegCM3 validation results for the 1981–2000 time span for a winter and a summer month, i.e. (a) January and (b) July. As a first step, box plots (Fig. 3a1, b1) showing the range of the wind speed values, as well as the 25 and 75 % quantiles, and the median are presented. RegCM3-10Km shows a satisfactory skill in representing the median of the wind speeds. Especially in Chania (Fig. 3iii), the model also captures the whole range of the values found for the examined period. RegCM3-10Km was able to simulate the outer edges of the boxes (25 and 75 % quantiles), even though this range is quite smaller than the ERA-Interim one in some of the cases. Furthermore, it was found that RegCM3-10Km simulations can also reproduce the mean value of the wind speed; generally, the differences are less than 1 m/s and thus insignificant for our analysis. The standard deviations of the wind speed time series are very similar to the ones of the ERA-Interim datasets (Fig. 3a1, b1). The occurrence frequency (%) of wind speeds was also calculated and is presented in Fig. 3a2, b2. Overall, the model manages to detect the ERA-Interim distributions and captures both the low and high classes, as well as the most frequent one (peak of the probability distribution function). The only exceptions correspond to Alexandroupoli and Kerkira in July (Fig. 3b2i, b2ii), where the model results underestimate the high frequency class. Nevertheless, most of the wind speed values (e.g. classes from 2 to 8 m/s) show a similar frequency of occurrence, especially in Alexandroupoli and Chania (Fig. 3a2i, a2iii).

The bias of wind fields between model and Era-Interim datasets could be attributed either to a low-skill representation of the dynamical and synoptic factors of atmospheric circulation or to the weakness of the model in capturing the complex terrain of the study domain. The plausibility of vertical (baroclinic) distributions of wind characteristics is strongly influenced by the preciseness of the orography representation. In our case, the simulation of *SLP* and pressure gradients by RegCM3-10Km is satisfactory as shown in the next paragraphs. Thus, one of the main reasons for biases in wind results is probably the accuracy of the model's topography scheme of the area.

Aiming to quantitatively assess the ability of the dynamically downscaled model to reproduce wind fields and decide on the essentiality of bias correction, we also calculated and used a model evaluation measure, i.e. the hit rate of percentiles (*HRP*) index (Schoetter et al. 2012). Namely, one computes the absolute differences between sorted (from 1st to 99th) percentiles of simulated and observed values. Then the *HRP* index is defined as the sum of the categorical fractions, i.e. differences compared to an allowed deviation. Schoetter et al. (2012) determined the values of allowed deviation for wind speed as 1 m/s. If *HRP* index (with range between 0 and 1) is greater than 0.95, then the model efficiently represents the regarded observation time series and the simulated dataset under examination does not need to be corrected for bias. *HRP* is independent of the variable under evaluation; thus, it is also used for the assessment of gridded *SLP* fields.

Therefore, we computed the *HRP* index (its total and its values for three percentile classes; 1st–33rd, 34th–66th and 67th–99th percentiles), in order to evaluate the RegCM3-10Km skill for the simulation of the entire wind speed time series and the low, medium and high ranges of wind speeds for the three selected areas. It was found that the model simulates wind speeds adequately, since *HRP* exceeds the limit of 0.95 and reaches the value of 1 both in total and in the three separate classes, especially in the case of Chania (Fig. 3a2iii, b2iii). The only exception is the case of Alexandroupoli during July where *HRP* is quite lower (0.76; Fig. 3b2i). However, this is due to inadequate representation of only the first class (low-speed winds), which is not important for the analysis of extreme waves and storm surges.

Regarding the mean *SLP* evaluation, the spatial distribution of monthly mean values for January and July (Fig. 4a, b) were computed from the ERA-Interim and RegCM3-10Km data in the area confined among 10° W–40° E and 30° N–50° N, during the 1981–2000 time span. Furthermore, the differences between the modelled and observed fields were mapped; the ranges of differences are also given in box plots (Fig. 4aii, bii). For the same spatial window and for all the grid points included in it, *HRP* index was calculated to evaluate the efficiency of model performance for *SLP* (Fig. 4aiii, biii). In the case of January, Fig. 4ai illustrates that both simulated (model) and reanalysis (ERA-Interim) maps have the highest *SLP* values at the southwestern part of the Mediterranean and the lowest at the northwestern one. The distribution of differences (Fig. 4aii) shows that the model underestimates *SLP* over the continental parts of Europe (negative values), while smaller positive values are observed over the Mediterranean and southeastern parts of the study domain. Median differences are less than 1 hPa and inner-quantile range (25–75 %) is between −1 and 4 hPa. The *HRP* index is higher than 0.95 for both the summer and winter indicative months over the entire Mediterranean Sea and a large part of it that covers the AIS, respectively (Fig. 4aiii, biii). It is also evident that the model adequately simulates the spatial distribution of the *SLP* values during July (characteristic summer month), with the lowest ones covering the eastern and southwestern parts of the spatial window examined; higher pressure values characterize central and western Europe. By examining the differences maps (Fig. 4aii, bii), it is found that RegCM3-10Km slightly overestimates *SLP* in the domain of study. The ability of the model in representing *SLP* values during the period 1981–2000 is confirmed by the use of the *HRP* index in almost all the parts of the domain of interest, where *HRP* is higher than the critical value of 0.95 (Fig. 4aiii, biii).

Hence, the simulated climatic data (*SLP* and winds) used as input for the specific aims of the present paper (i.e. climate simulations of storm surges, waves and their extremes) were considered to be in no imperative need of bias correction and that the dynamically downscaled RegCM3 implementation could efficiently reproduce wind and *SLP* characteristics in the AIS.

3.2 The wave model

A simulation scheme based on the SWAN wave model's version 40.91 (Booij et al. 1999, Ris et al. 1999) was developed for the wave climate simulation. SWAN is a "free" and open-source, third-generation (Young 1999) phase-averaging wave model that solves the spectral action balance equation (Komen et al. 1994; Holthuijsen 2007). The model simulates wave generation by wind, wave propagation, shoaling, refraction and diffraction, wave dissipation due to whitecapping, bottom friction and depth-induced breaking, interaction with obstacles, etc. (SWAN 2012).

The scheme uses one stage of nesting, leading to two simulation levels. Level I includes the entire Mediterranean Sea with resolution 0.2° × 0.2° and level II includes an east-central part of the Mediterranean with resolution 0.05° × 0.05° (Fig. 2b). The bathymetry is based on the General Bathymetric Chart of the Oceans (GEBCO, Becker et al. 2009) for both levels. Level I simulation was forced by the RegCM3-25Km wind fields and level II simulation by the downscaled RegCM3-10Km fields (Section 3.1). SWAN was executed in nonstationary mode with a 10-min time step and the Backward-Space-Backward-Time numerical integrator was used in both levels of implementation (SWAN 2012). The basic configurations of the simulations are summarized in Table 1. The output of the scheme consisted of the SWH, H_s, mean (energy) wave period, T_{-10}, mean zero-crossing wave period, T_{02}, mean peak spectral wave period T_p (for level II) and mean wave direction for all "wet" points of the computational grids at 3-h intervals. The main reason for using SWAN instead of other models is that the finest simulation level (level III; results in selected coastal areas not presented herein) consisted of additional nested, nearshore, high-resolution simulations, where SWAN has improved physics features

compared to other third-generation wave models and is known to perform better than them. In order to reduce the simulation scheme complexity, SWAN was also implemented in the Mediterranean and AIS simulations (levels I and II, respectively).

The simulation scheme was validated through systematic comparisons with an operational WAM (Cycle 4) implementation (courtesy of the Atmospheric Modelling and Weather Forecasting Group, University of Athens; Galanis et al. 2012), due to unavailability of field data from buoys in the area. Initial comparisons indicated a negative bias in the mean wave periods predicted by SWAN (also documented in Rogers et al. 2003, Van der Westhuysen et al. 2007, SWAN 2012). Modifying the whitecapping dissipation term parameterization ("delta" in "GEN3" command equal to one) removed the aforementioned bias and the two models show good agreement (Fig. 5a–c). For further validation against measurements, the model was also driven with altimeter reanalysis winds (blended with model data) for the period 21 January–19 March 2009 (~15,000 data pairs), and compared with corresponding H_s altimeter measurements obtained from AVISO (http://www.aviso.oceanobs.com/) (Fig. 5d). Model output displays quite acceptable agreement with the satellite altimetry measurements.

3.3 The storm surge model

For the storm surge simulations, the GreCSSM implementation was developed in order to numerically solve the depth-averaged shallow water equations in two horizontal dimensions. GreCSSM simulates the meteorologically induced sea-surface variations over the AIS on a 1/20° × 1/20° (~5 km) horizontal grid (parameterizations in Table 1). Six-hourly atmospheric forcing, i.e. winds at 10 m and *SLP* fields, was provided by RegCM3 simulations for the entire study period (1951–2100). GreCSSM domain (level II) has two sea boundaries one-way nested to MeCSSM (level I: 1/10° × 1/10°), implemented over the entire Mediterranean Sea (Androulidakis et al. 2015).

The output of GreCSSM consists of atmospherically induced sea level variations, namely *SLH*. We investigated characteristic values of the largest *SLH* per year, using the Storm Surge Index (*SSI*; Conte and Lionello 2013). *SSI* is defined as the average of the three highest independent storm surge maxima per year. Only events separated by at least 120 h (estimation of the maximum duration of a storm in the AIS) are considered as independent storm events. The *SSI* was calculated at specific locations (study stations in Fig. 2c), for both simulated and observed time series, along with the corresponding Error Index (*EI*):

$$EI = \left(\overline{SSI}_{mod} - \overline{SSI}_{obs}\right) \Big/ \sqrt{\left(\sigma^2_{SSI_{mod}} + \sigma^2_{SSI_{obs}}\right)\Big/2} \qquad (1)$$

where the overbar denotes mean *SSI* values over the comparison period, as derived from modelled (mod) and observed (obs) field data, and σ is the standard deviation of the inter-annual variability of *SSI* time series for each station. *EI* is positive when the model overestimates the amplitude of the sea level against field data, obtained from the Hellenic Navy Hydrographic Service (HNHS; http://www.hnhs.gr/portal/page/portal/HNHS). The field data from in situ observations (by digital gauges in Alexandroupoli, Chios and Lefkada; by analogue gauges in Thessaloniki and Heraklion) are daily averaged *SLH* values that were filtered in order to (a) remove the astronomical tide signals with T_Tide (Pawlowicz et al. 2002) and (b) exclude long-term (>30 days) oscillations of the sea level (Conte and Lionello 2013) due to steric effects, i.e. large-scale, low-frequency, thermohaline fluctuations and/or total mass variations of the Mediterranean basin (Carillo et al. 2012). The *SLH* records have minimal gaps in their time series and cover the 18-year period of 1995 to 2012; thus, they refer to the last 6 years (1995–2000) of the reference period and also cover the incipient 12 years (2001–2012) of the current period.

Figure 6 presents the evaluation of the GreCSSM simulations based on comparisons of model results against field observations at five stations. In the upper graphs, comparisons are based on averaged intra-annual maxima, i.e. mean *SSI*, and its *EI* followed by box plots of *SSI* (lower graphs). Comparisons support the good performance of the model, with rather small errors for the averaged *SSI* feature, i.e.

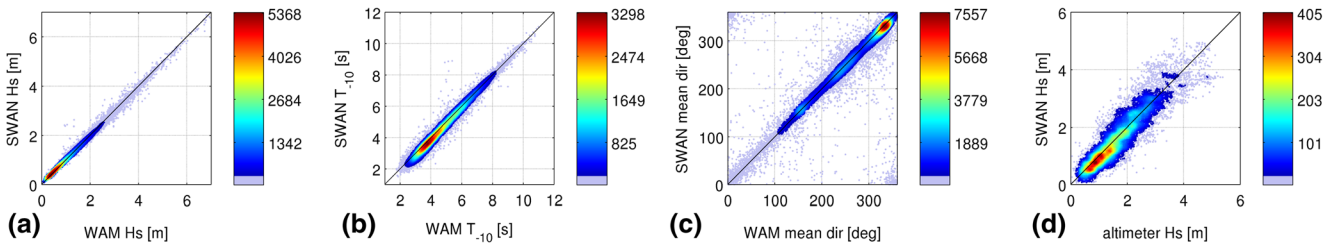

Fig. 5 Scatterplots of **a** H_s, **b** T_{-10} and **c** mean wave direction as calculated by SWAN and WAM models, using identical input ($4 \cdot 10^4$ data pairs); **d** scatterplot of H_s altimeter measurements vs. SWAN model calculations forced by reanalysis input (~$1.4 \cdot 10^4$ data pairs). *Colour* corresponds to point density in accordance with the *colour bars*

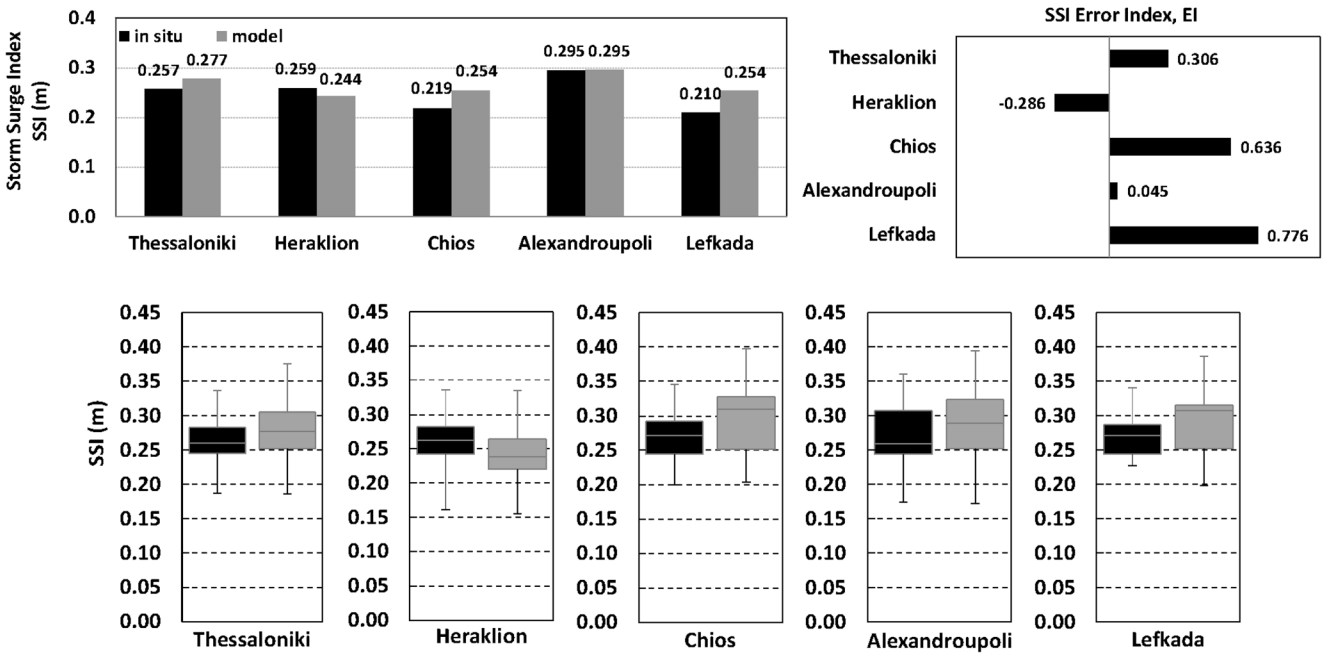

Fig. 6 Validation of GreCSSM model output (*grey colour*) against field (in situ) observations (*black colour*) at five Greek stations covering an 18-year period (1995–2012). Comparisons are based on mean *SSI* (m) and *EI* (*upper left* and *right graphs*, respectively) and box plots of *SSI* presenting the minima, maxima, medians and 1st and 3rd quartiles of *SSI* (*lower graphs*)

absolute *EI* is less than 0.8 in all stations. The most reliable model results, in terms of annual *SLH* maxima (*SSI*), are found in the regions of the North and South Aegean (Alexandroupoli and Heraklion) followed by the Thessaloniki and Chios stations. The largest simulation error (yet acceptable, $EI \approx 0.78$) is traced in the Ionian Sea station (Lefkada), which lies near the western boundary of the computational domain. The box plots show that the 18-year minima of *SSI* are well estimated by our model in all stations, while the 18-year maxima of *SSI* are overestimated everywhere except from Heraklion, where they are accurately reproduced compared to in situ values. The same analogy applies to the 18-year 1st and 3rd quartiles of the *SSI* time series.

Figure 7 presents the inter-annual (18-year period) maxima, i.e. mid- and high-order (80th and 99th) percentiles of *SLH* (upper graphs), together with the box plots for the entire time series of modelled and observed *SLH*. The mid- and high-order (80th and 99th) percentiles of *SLH* show that modelled values are quite close to the field data, which is satisfactory in terms of GreCSSM evaluation for climatic simulations of extremes. The North Aegean station of Alexandroupoli ($EI = 0.045$) shows the best results compared to all other regions examined. The higher resolution of the GreCSSM simulation slightly improved the results of *SLH* fields in the AIS, as shown by Makris et al. (2015), producing smaller errors over the Greek areas in comparison with the coarser MeCSSM simulation presented by Androulidakis et al. (2015). The box plots reveal that the 18-year quartiles and maxima of *SLH* are very well estimated by our model in all stations, while the 18-year minima of *SLH* (representing negative surges unimportant for the purposes of the present study) are underestimated by 10–15 % compared to in situ values everywhere except from Lefkada. Moreover, the probabilities of exceedance of coherent and intense events P_{coh} and P_{int} (%) are also shown in the lower graphs of Fig. 7. P_{coh} and P_{int} are heuristically defined statistical measures for coherent (coh) and intense (int) *SLH* events (Jaffe and Sallenger 1992, Cox and Kobayashi 2000), which exceed certain critical (threshold) values, namely $SLH_{coh} > (m + \sigma)_{SLH}$ and $SLH_{int} > (m + 2\sigma)_{SLH}$; m is the mean of the *SLH* time series (1995–2012) and σ is the corresponding standard deviation. Simulated values of P_{coh} correlate very well with the ones corresponding to field observations in all stations. The simulated frequencies of intense events are slightly overestimated compared to the field data, yet differences are very small, i.e. in the order of 0.4~0.9 %. Conclusively, the results of the model implementation verify the overall good performance of GreCSSM in terms of both intra-annual and inter-annual maxima for the evaluation period.

Furthermore we calculated the *HRP* index for the entire 18-year *SLH* time series in order to examine if bias correction is necessary for modelled storm surge results. The allowed deviation was taken equal to half the average standard deviation of the modelled and in situ *SLH* time series, i.e. $(\sigma_{SLHmod} + \sigma_{SLHobs})/2 \approx 4$ cm that is 5–10 % of average observed SLH_{max}. It was found that *HRP* ranges from 0.95 to 1 in all Greek stations; therefore, bias correction was not imperative for modelled *SLH*.

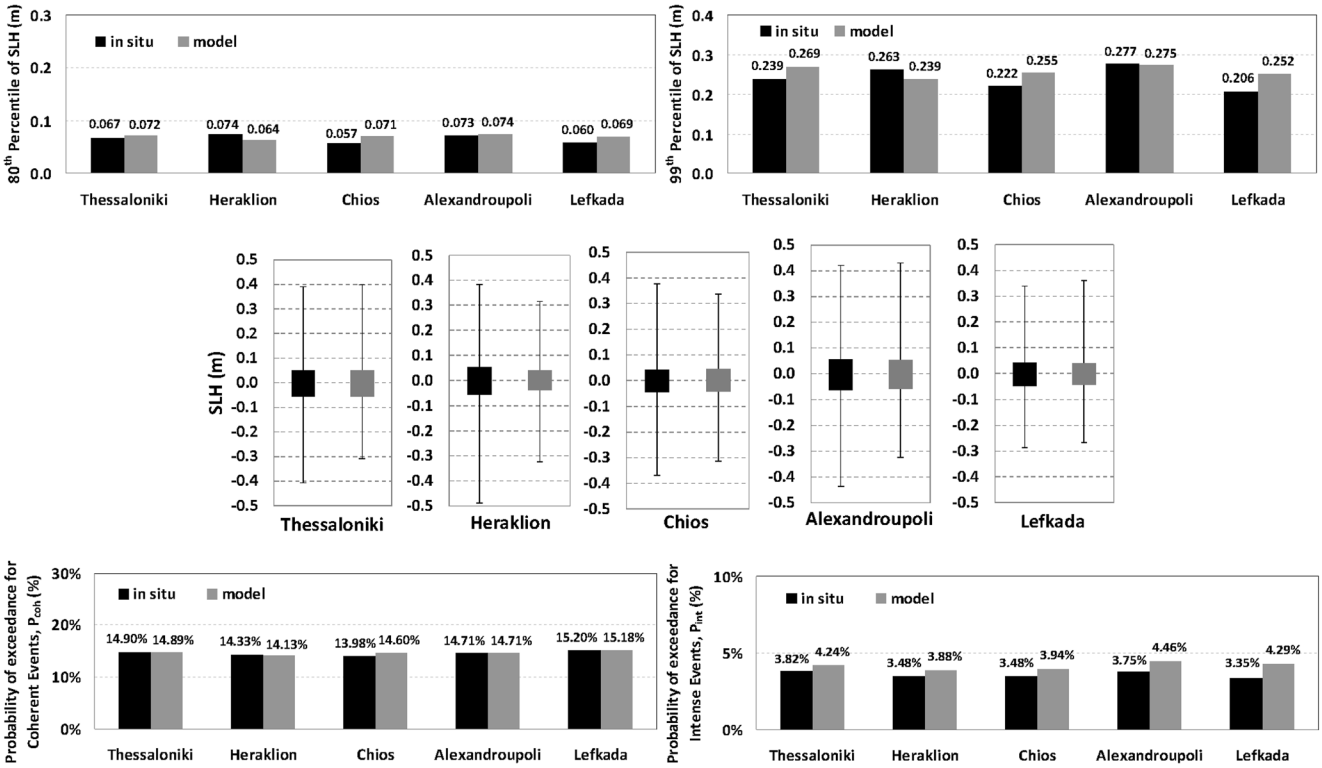

Fig. 7 Validation of GreCSSM model output (*grey colour*) against field (in situ) observations (*black colour*) at five Greek stations covering an 18-year period (1995–2012). Comparisons are based on mid- and high-order percentiles (80th and 99th; *upper left* and *right graphs*, respectively) of *SLH* (m), box plots presenting the minima, maxima, medians, 1st and 3rd quartiles of *SLH* (mid graphs) and probabilities of exceedance of coherent and intense events P_{coh} and P_{int} (%) (*lower left* and *right graphs*, respectively)

3.4 Extreme value analysis

To analyse the marine climate extremes in eight areas of focus prone to coastal flooding (Fig. 2c), annual and monthly maxima of H_s and *SLH* at a number of grid points are used. Each area is divided in homogeneous parts in terms of the distribution of extremes, utilizing the homogeneity measures of Hosking and Wallis (1997) for the extracted maxima of H_s and *SLH*. Distinct grid points, representative of each homogeneous part, are selected and the respective extreme samples are further analysed. While all eight areas appear to be acceptably homogeneous in terms of their *SLH* extremes, H_s extremes impose the division of four areas in two homogeneous parts. Therefore, two grid points are selected for each of the marine areas of Alexandroupoli (northern Aegean), Lesvos (east-central Aegean), Parga and Kerkira (central and northern Ionian, respectively), whereas a single representative grid point is selected for the rest of the eight marine areas.

The wave height and storm surge extremes are studied using the univariate Extreme Value Theory (EVT) for 50-year time intervals (1951–2000, 2001–2050 and 2051–2100). The family of univariate extreme value distributions includes models for maxima of appropriately defined groups (e.g. distribution functions for annual or monthly maxima), as well as models for exceedances over high enough thresholds, i.e. Peaks Over Threshold (POT) models. The former correspond to the generalized extreme value (GEV) distribution function (Coles 2001) with parameters μ (location), σ (scale) and ξ (shape). To incorporate the seasonal component in the stationary GEV distribution, each parameter can be represented as a harmonic function of time of the form presented by Menéndez et al. (2009). The optimum number of harmonics used in each of the three parameters is assessed by minimizing the Akaike criterion (AICc) with correction for small sample sizes (Hurvich and Tsai 1989), as well as by the deviance statistic function D (Coles 2001).

When considering processes with time-dependent properties, the return level (z) is perceived as the quantile of the fitted distribution at a certain time of a given year; therefore, it is assumed to vary with time, i.e. $z_p(t)$ for an exceedance probability p. Annual return levels, z_p, corresponding to a certain exceedance probability, p, can be calculated by iteratively solving the Cumulative Distribution Function (CDF) of the GEV distribution, expressed as a function of time-varying parameters and quantiles integrated over an entire year (Menéndez et al. 2009). Results for different return periods, $T = 1/p$, can be presented in a return level plot for the interpretation of stationary extreme value models.

3.5 Bias correction for marine characteristics

Simulations of the marine climate using RCM forcing may be subject to bias, which represents the error component of the climatic model (Haerter et al. 2011). Among the bias correction techniques, quantile mapping methods are indicated as the most efficient, even for the most extreme part of the distribution of the studied variables (Themeßl et al. 2012). The methods used in the present work include both parametric (linear, polynomial, scale or power transfer functions) and non-parametric (cubic smoothing splines) quantile-quantile transformations (Gudmundsson et al. 2012). In the present study, bias correction is considered necessary only for the analysis of wave height extremes; the *HRP* index for *SLH* is found to be over 0.95. The main reason is that significant differences are noticed between the tails of the CDFs of the SWAN results and observations or WAM simulations of wave heights. Because of the very short continuous series of observed data of wave heights in the areas of interest, only simulated SWH fields are utilized for bias correction purposes. Therefore, wave predictions by the WAM model forced with the non-hydrostatic model SKIRON weather forecast input (Kallos et al. 1997, Papadopoulos et al. 2002) are used for all study areas of focus. The modelled data cover a period of ten years and are provided with an hourly time resolution. The horizontal spatial resolution of SKIRON and the wave prediction model WAM is 0.05° × 0.05° matching level II of our SWAN simulations; all selected SWAN grid points are fitted to the ones of WAM. Some examples of post-processing (bias correction) of wave and storm surge data in the literature can also be found in Marcos et al. (2011), Benetazzo et al. (2012) and Charles et al. (2012). According to Charles et al. (2012), even in case studies of using climatic parameters as forcing input in e.g. wave models, it is suggested that the bias correction (if unavoidable) should be applied only to the wave fields and not to the simulated wind data. This kind of practice could prevent crucial modifications of the local atmospheric circulation patterns that are essential to RCM simulations, and thus was also followed herein.

4 Present climate and future projections of atmospheric and marine characteristics

4.1 Analysis of wind and sea level pressure fields

SLP and wind (speed and direction) fields simulated by RegCM3 are used in the present analysis for the study of the AIS climate. Results from the model's simulations are compared with the general atmospheric circulation patterns in the Mediterranean and the prevailing wind patterns in the AIS. The future projections are used for the assessment of the possible changes in the characteristics of the *SLP* and wind patterns.

4.1.1 Sea level pressure

RegCM3 quite satisfactorily simulates the general atmospheric circulation over the Mediterranean. Figure 8 shows the high-pressure system above the Iberian Peninsula and western Europe due to the extension of the Azores high, as well as its displacement throughout the year. Similarly to the Azores high, the extension of the Icelandic low is quite evident in northwestern Europe with low pressure values (Fig. 8a1). The European and the Balkan Peninsula anticyclones are combined into a continuous high pressure system above central Europe and the Balkan Peninsula, respectively. Moreover, the Siberian high pressure system during the cold period is modified to the Asian thermal low during the warm period. In the southern part, the West African heat low is apparent during summer with low pressure values above West Africa. A southerly migration of the West African heat low is also observed in the cold period.

For the current period (2001–2050), a reinforcement of high pressure values in western Europe and the Iberian Peninsula and a weakening of low pressure values northwest of Europe are observed during January. Analogous were the results of Santos et al. (2007), who used a different RCM and found that a reinforcement and a swift to the east is expected for the Azores high (southern pole of NAO index) during winter in the future. There is no significant change of the pressure gradient above the Balkan Peninsula, South Asia and western Africa (Fig. 8b1). In spring, and especially in April, the attenuation of low pressure values northwest of Europe and high pressure values above West Africa and the Iberian Peninsula reveal the displacement of the Azores high (not shown). High pressures are enfeebled in central Europe during summer, while low pressures are decreased in Asia, Middle East and West Africa, i.e. the Asian thermal low and the West Africa heat low are respectively deeper. These findings are in agreement with Anagnostopoulou et al. (2014), who showed that there is a strengthening of the two aforementioned synoptic centres for the future period. This is quite obvious in July (Fig. 8b2). This atmospheric circulation system results to moderate Etesian winds over the Aegean Sea, due to the moderate pressure gradient. However, there is a strengthening of the high pressure system over central Europe and the Balkan Peninsula in August (not shown). Furthermore, the positive centre extents from western to central Europe during autumn, mainly during October (not shown). Similar results are found for the future period (2051–2100) (Fig. 8c1, c2). Differences of pressure gradient between the future and the reference period are more intense compared with the ones between the current and the reference period (Fig. 8b1, b2). In particular, small differences are

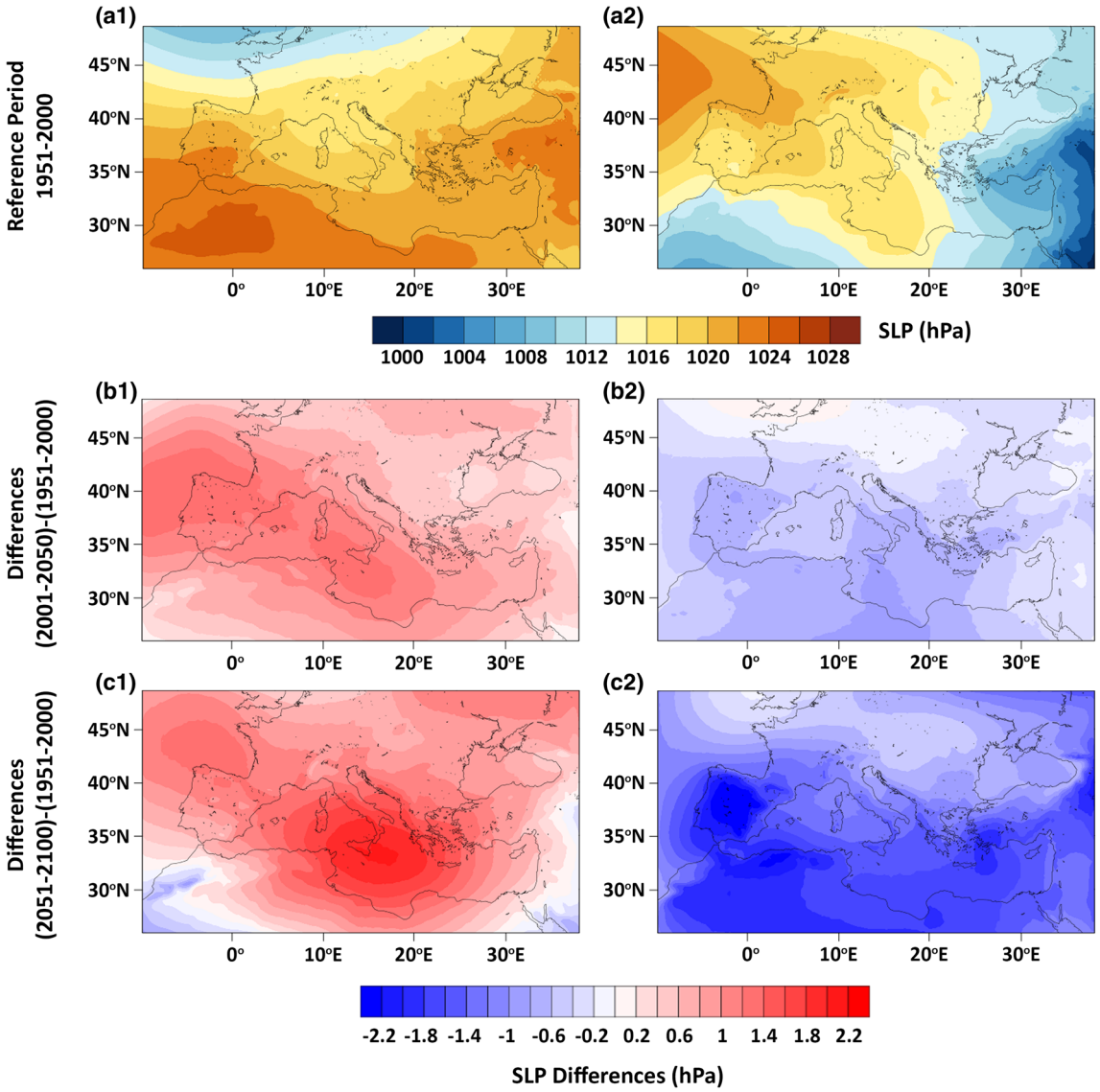

Fig. 8 **a** Mean *SLP* (hPa) maps for the reference period (1951–2000). Maps of differences for mean *SLP* (hPa) **b** between the current period (2001–2050) and the reference period; **c** between the future period (2051–2100) and the reference period for (*1*) January (characteristic month of cold period) and (*2*) July (characteristic month of warm period)

mainly evident in June, when a rise of high pressures is evident at the northwest of and above central Europe. Eventually, a reinforcement of high pressures is noticeable above Greece (Aegean Sea) and the Middle East in December.

4.1.2 Wind climate

In the North Aegean Sea, the wind direction does not vary significantly throughout the year and is mainly northeastern (Fig. 9a1, a2). The wind speeds range between 7 and 8 m/s in the cold period and 5 to 7 m/s in the warm period. In the central Aegean Sea, the wind speeds increase slightly, while generally winds become northerly throughout the year. The prevailing wind direction in the South Aegean Sea is mainly northern during the year, apart from spring, during which the winds blow from the West (not shown). The winds are steadily blowing from the Northwest in the Southeast Aegean. In the Ionian Sea, winds seem to gradually shift from westerly to northerly for all three 50-year periods (Fig. 9a1, a2; b1, b2; c1, c2). In the southern AIS the wind velocities are consistent during the year as they range from 7 to 9 m/s; there is an exception during summer (*sc.* July) when wind speeds in the Ionian Sea are not that intense.

Changes of the 50-year patterns of wind speed and direction in the AIS are computed with respect to the reference period. The wind directions in the first half of the twenty-first century are similar to the ones of 1950–2000. During the warm period of the year, winds in the South Aegean Sea

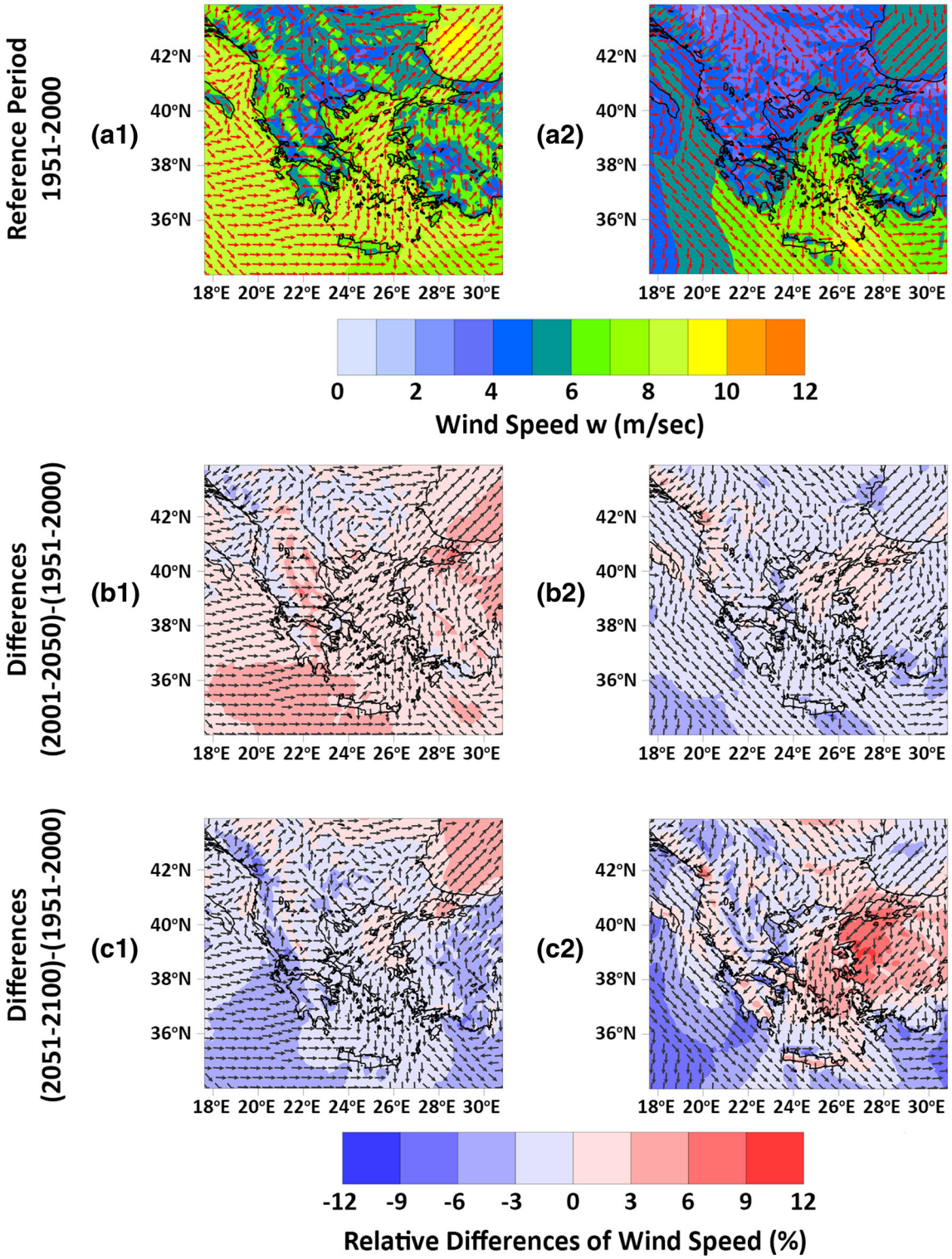

Fig. 9 **a** Mean wind speed (m/s) and prevailing wind directions maps for the reference period (1951–2000). Maps of prevailing wind directions and relative differences for mean wind speed (%) **b** between the current period (2001–2050) and the reference period; **c** between the future period (2051–2100) and the reference period for (*1*) January (characteristic month of cold period) and (*2*) July (characteristic month of warm period)

are mainly blowing from the West, whereas in the cold period of the year the prevailing winds shift to northerly. January is characterized by a slight increase of wind speed across the study area (Fig. 9b1) that reaches 5 % in the Ionian Sea, whereas wind speeds decrease in the major part of the study area during the rest of winter. During the warm period, there are obvious differences in wind patterns between the Ionian and the Aegean Seas. The relative differences between wind

speeds are mainly negative (Fig. 9b2) during summer (*sc.* in July). Mclnnes et al. (2011) used numerous general circulation models and also found that a reduction of the mean wind speed is expected during winter in the Ionian and the southern Aegean Sea towards the end of the twenty-first century, while they estimated an increase of mean wind speed over Greece during summer.

Similar results are derived regarding the wind directions (Fig. 9c1, c2) for the future period. In January, and also during the entire winter season, wind speeds decrease across the study area (Fig. 9c1). During summer and spring, the wind speeds increase in the Aegean Sea (e.g. more than 10 % in June; not shown). Negative values are observed in the Ionian Sea, which are more intense in July, i.e. about −10 % in the southwestern Ionian Sea (Fig. 9c2). A decrease is also detected in the South Aegean Sea for the warm period (July). In autumn, a reduction of wind speeds is noted across the study area, which reaches 10 % in the Ionian Sea apart from September, during which a reinforcement of wind speed (about 10 %) is observed in the central and southern Aegean Sea (not shown).

For a more detailed investigation of the wind patterns, the wind roses for three subregions are presented; one representative grid point per selected subregion is analysed. The colour scale in the wind roses (Fig. 10) corresponds to the magnitude of the wind velocity, which ranges from 1 to 16 m/s and the numbers in the axis are percentage of cases with a certain wind direction. In the North Aegean Sea, there are two main (opposite) wind directions, namely the northeastern and southern-southwestern. Southerly to southwesterly winds are observed only during winter (January) and spring (not shown), whereas northeasterly winds are observed all through the year (Fig. 10a1, a2). The wind speeds range from 7 to 10 m/s with 4 % of the cases varying from 10 to 13 m/s.

On the contrary, the occurrence frequency of wind speeds between 7 and 10 m/s is about 14 % in summer (*sc.* July). Similar results are derived for the current and future periods (Fig. 10b1, b2, c1, c2). In the South Aegean Sea, the main winds are of a northern-northeastern component during the cold period (January), nevertheless there are many cases that shift from westerly-northwesterly to southwesterly directions in all three periods (Fig. 10a3, b3, c3). Regarding the warmer period of the year (July), the winds shift from northerly to northerly-northeasterly in all three periods (Fig. 10a4, b4, c4). The main observed wind velocities belong in the class of 7–10 m/s. The Ionian Sea is affected by the winds that blow from North, West and South, due to the presence of the land and the western orientation of the coastal zone (Fig. 10a6, b6 and c6).

4.2 Analysis of mean and extreme waves

The results of the SWAN simulations are presented and discussed concerning the mean and extreme wave climate of the AIS for the reference, current and future periods. Concise information of the Mediterranean (level I) wave field simulations is also presented.

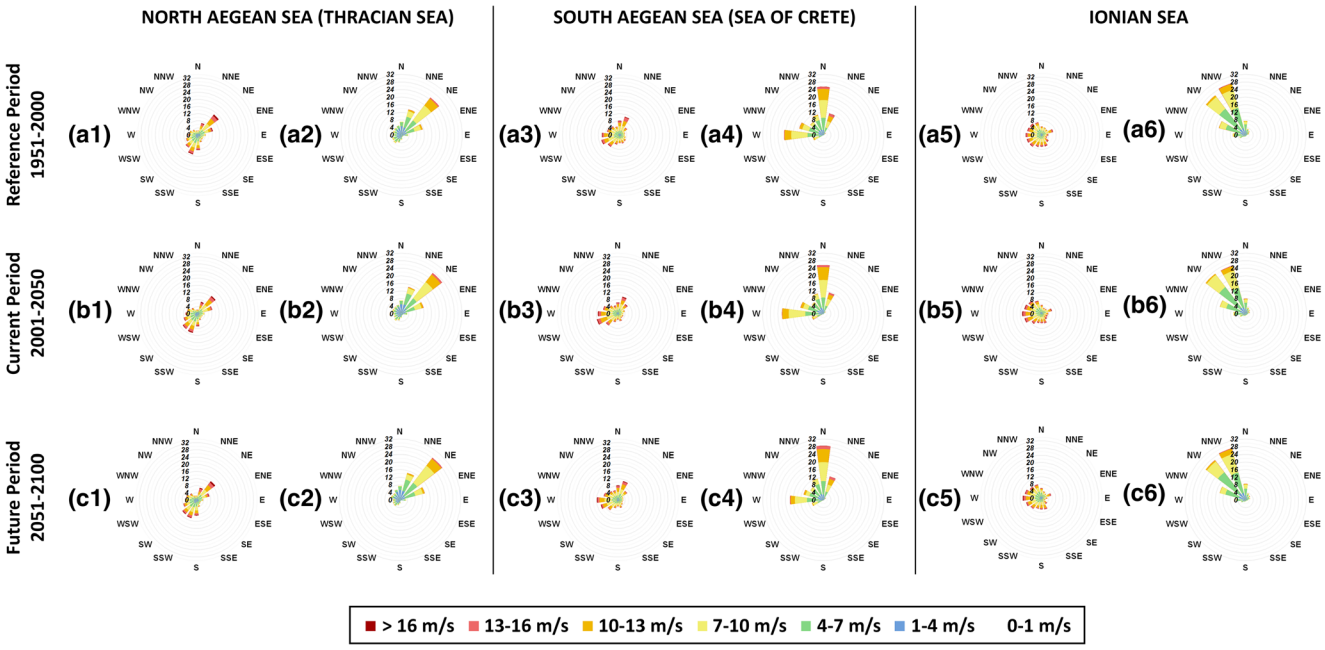

Fig. 10 Wind roses for the three areas denoted by *blue stars* in Fig. 2e, i.e. of the North Aegean Sea, the South Aegean and the Ionian Sea; **a** for the reference period (1951–2000), **b** for the current period (2001–2050) and **c** for the future period (2051–2100) during the cold period (*1*, *3*, *5*) and during the warm period (*2*, *4*, *6*) of the year

4.2.1 Analysis of mean wave regime

The mean wave climate results have been subdivided in two parts: a high-energy season (months November to April) and a low-energy season (months May to October), based on the mean-monthly wave energy in the east-central Mediterranean. Results for the entire Mediterranean basin (level I; not shown) lead to estimations of a general incipient increase and gradual decrease of the mean H_s field in the twenty-first century (current and future periods), compared to that of the reference period; lowest values appear during the second half of the twenty-first century. This effect is stronger in the three subregions of the AIS, where the H_s difference between the future and the reference period is of the order of 0.25 m, for the high-energy season. The seasonal patterns of mean-monthly H_s and T_{-10} for the three periods at three characteristic offshore (western, central and eastern) locations in the Mediterranean Sea show a strong correlation between the two and a slight reduction of mean H_s and T_{-10} during the high-energy months especially for 2051–2100. The values of wave characteristics reveal a firm pattern of west-to-east decrease. In general, the forms of the seasonal patterns are almost invariable for the three periods in all locations.

Level II results for the 50-year mean and averaged annual maxima of the H_s field in the AIS are presented in Figs. 11 and 12, respectively. An overall slight decreasing trend of mean H_s is also observed for the high-energy season in level II (Fig. 11, upper row). The Ionian and Libyan Seas are significantly affected, including the regions near the Greek mainland; a similar tendency, yet with weaker magnitude, is noticeable in the central part of the North Aegean Sea and the region north of Crete. Results for the low-energy season are also shown in Fig. 11 (lower row). The 50-year changes of mean H_s fields are reversed for the warm period of the year. In the Ionian and the North Aegean Seas, the fields are seemingly invariable through time. However, in contrast to the general trend, an increase of the mean H_s (up to 0.20 m locally) is observed in the southeastern and central Aegean Sea for the future period, especially at the parts surrounding the island group of Cyclades and near the Crete-Karpathos strait. This is associated with the corresponding increase of the Etesian winds at the central part of the Aegean in the same period. The latter is the main probable cause for the change of patterns in fields of H_s annual maxima (Fig. 12, upper row). Specifically, $H_{s,max}$ values are estimated to intensify in the northern and central

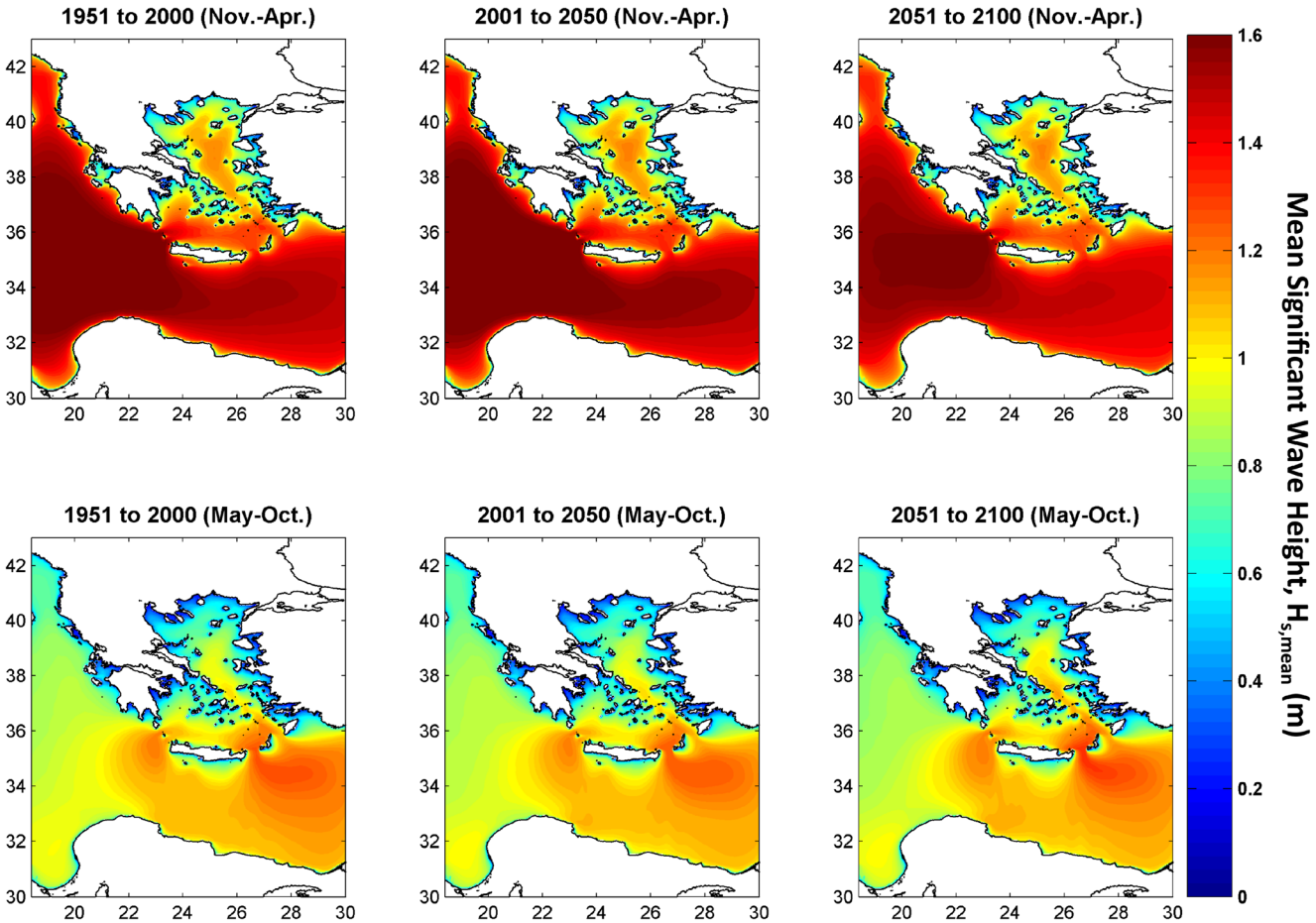

Fig. 11 Temporal mean of SWH, $H_{s,mean}$ (m), during high-energy (*upper row*) and low-energy (*lower row*) months over the AIS for 50-year time intervals, i.e. the reference (*left graphs*), current (*central graphs*) and future (*right graphs*) periods

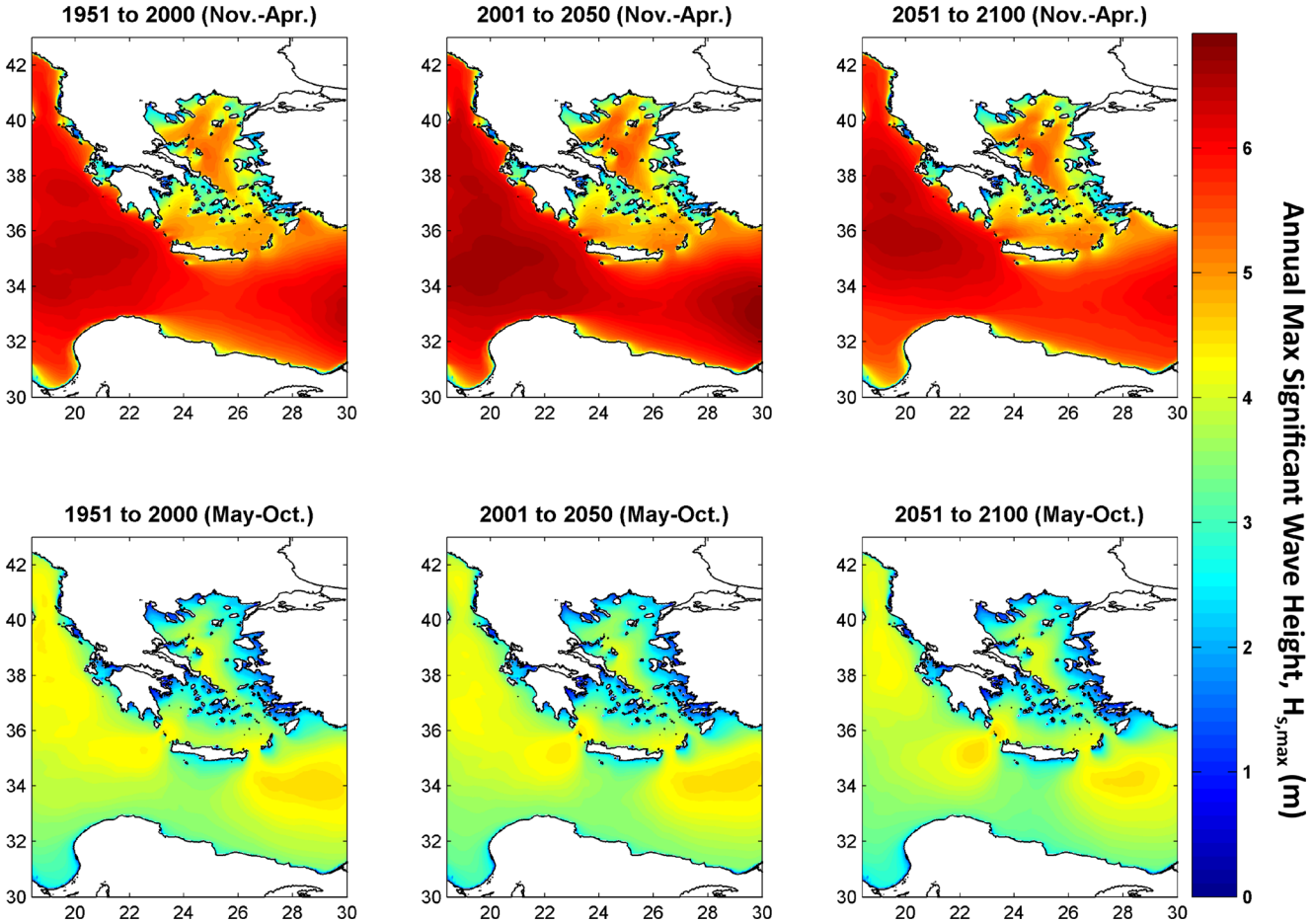

Fig. 12 Temporal mean of annual maxima of SWH, $H_{s,max}$ (m) and during high-energy (*upper graphs*) and low-energy (*lower graphs*) months over the AIS for 50-year time intervals, i.e. the reference (*left graphs*), current (*central graphs*) and future (*right graphs*) periods

parts of the Aegean Sea, with smaller values in southern AIS. There is also a clear increase of H_s yearly maxima in the Ionian and Libyan Seas during the current period and a consequent attenuation in the second half of the twenty-first century, following the changing patterns of mean H_s. $H_{s,max}$ fields are mainly time-invariant during the low-energy seasons in the entire study area.

The seasonal patterns of mean-monthly H_s and T_{-10} for the three periods at three characteristic offshore stations in the North Aegean, South Aegean and Ionian (denoted by blue stars in Fig. 2e) are presented in Fig. 13a (left panels). Local probability density functions (PDFs) of the wave parameters (H_s and T_{-10}) at the same stations are shown in Fig. 13b (right panels). PDFs are computed by fitting a log-normal distribution to the data. The shapes of seasonal distributions of wave heights and periods remain unchanged unlike their magnitudes. The peaks of modelled energy spectra seem to shift to higher frequencies and smaller powers in the twenty-first century. Thus, the mean field patterns are estimated to give slightly smaller and shorter waves in the AIS from the reference to the current and future periods; this follows the general storminess attenuation trend.

The polar probability plots for the mean wave directions (not shown), produced via kernel density estimation utilizing wrapped-Gaussian kernels (Athanassoulis and Belibassakis 2002), show that the probability of waves coming from Northeast is gradually increased during the low-energy season of the current period and more keenly for the future period.

4.2.2 Analysis of extreme waves

Wave height extremes are analysed in eight selected areas of the AIS prone to coastal flooding (Fig. 2c), using the extreme value techniques presented in Section 3.4, following the bias correction of wave data and extracting monthly SWH maxima (Section 3.5). Only events separated by at least three days (estimation of the representative duration of a storm and consequent rough sea state in the AIS) are considered as independent ones. 26 nonstationary GEV distribution functions with up to two harmonic functions in all model parameters are fitted to the data of each area and period, and the best-fit model is conditionally selected.

The study areas in the subregions of the AIS, viz. in the Ionian, the northern and the southern Aegean Seas, are

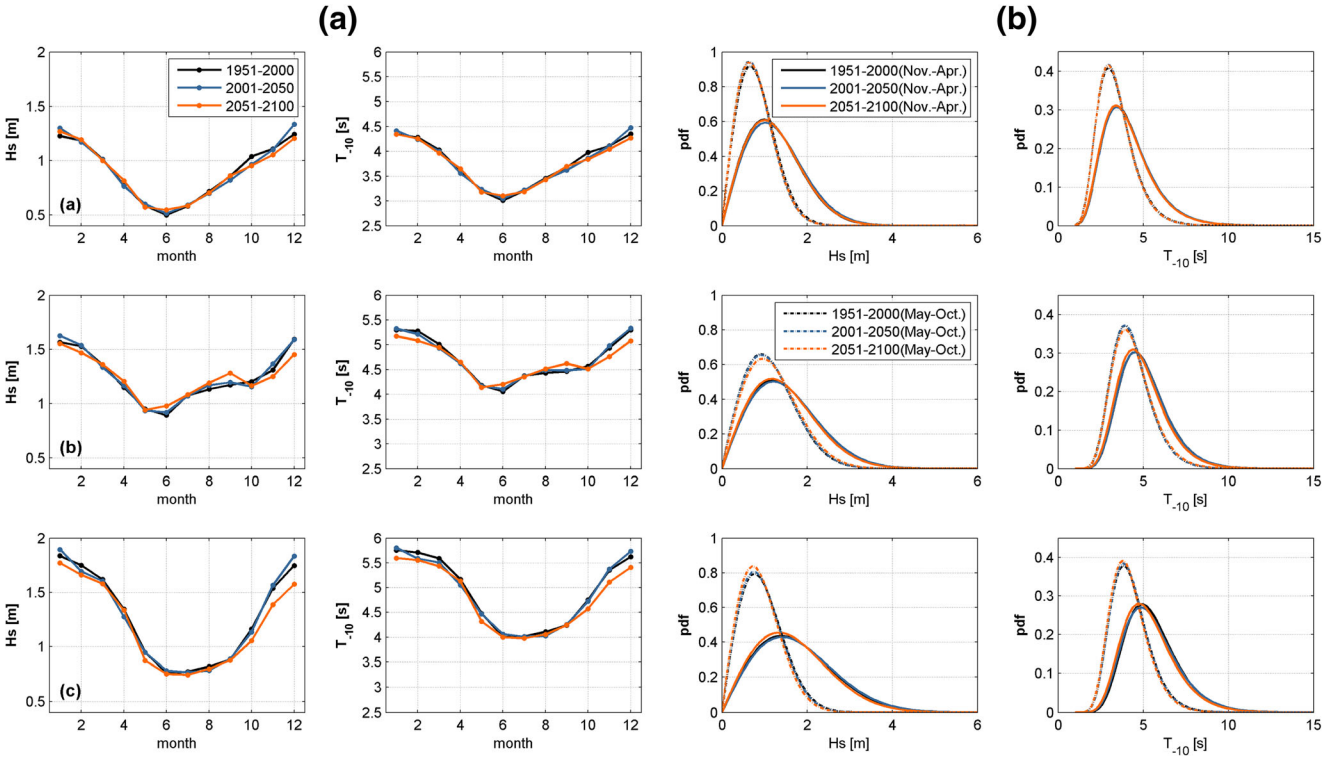

Fig. 13 **a** Seasonal patterns of H_s (m) and T_{-10} (s) at three offshore stations in the North Aegean, South Aegean and Ionian from *upper to lower graphs* denoted by *blue stars* in Fig. 2e (*left-panel graphs*); **b** probability density functions (pdf) for H_s and T_{-10} for the high-energy (*full lines*) and low-energy (*dashed lines*) seasons at the same three stations (*right-panel graphs*); all distributions (*coloured lines*) refer to 50-year time intervals of the reference, current and future periods

characterized by distinct structures of the nonstationary GEV distribution function. More specifically, the areas of Chania and Heraklion present similar model structures with one harmonic in the location and scale parameters for the reference period. Two and one harmonics in the location and the scale parameters are used, respectively, for the reference and future periods. The majority of the selected models for wave height extremes analysed in the three study areas of the Ionian Sea (Parga, Kyparissia and Kerkira) present one harmonic in the location parameter and two harmonics in the scale parameter of the GEV distribution function for all three periods. For the respective areas in the North Aegean Sea (Alexandroupoli, Katerini and Lesvos) harmonic functions appear also in the shape parameter of the GEV modifying the tail behaviour of the wave height extremes within the year.

Figure 14 presents the 98 % wave height quantile levels, corresponding to a return period of 50 years, in a time interval of one year and for all three periods considered in the marine areas of Alexandroupoli, Heraklion and Kyparissia (Fig. 2c). The maximum likelihood estimates (*MLEs*) of the quantiles are represented with a solid line whereas the shaded areas correspond to the 95 % confidence intervals estimated using the delta method. The monthly maxima of each sample in chronological order are also included as points. For the marine area of Alexandroupoli, peaks in extreme wave height quantiles appear at the end of autumn or within the winter season for the reference and the current period. Apart from the highest peak in November, a second peak is also apparent in mid-spring season for the future period. The auxiliary peak is accompanied with increased uncertainty in extreme H_s estimates. The respective H_s quantile levels in the other study areas of the North Aegean Sea (Katerini and Lesvos; not shown) reveal peaks in the middle or at the end of the winter period for all three periods considered. For the marine area of Heraklion, the 98 % wave height quantiles present single peaks in the middle and at the end of the winter season for the reference and the other two (current and future) periods, respectively. For the marine area of Kyparissia and the rest of the study areas in the Ionian Sea (not shown), the highest extreme H_s quantiles appear mostly in the winter season for all three periods. A prolonged peak period for wave height extremes, covering almost four months, is noticed for the future period.

Figure 15 shows the annual wave height return levels of return periods between 2 and 200 years in the marine areas of Alexandroupoli, Heraklion and Kyparissia for the three 50-year periods, shown in successive pairs (1951–2000 with 2001–2050, 2001–2050 with 2051–2100). In the marine area of Alexandroupoli, an increase in the severity of extreme wave events is obvious in the current period. This increase in *MLEs* of extreme wave heights exceeds 14 % for a return period of 50 years, compared to the reference period conditions. Higher

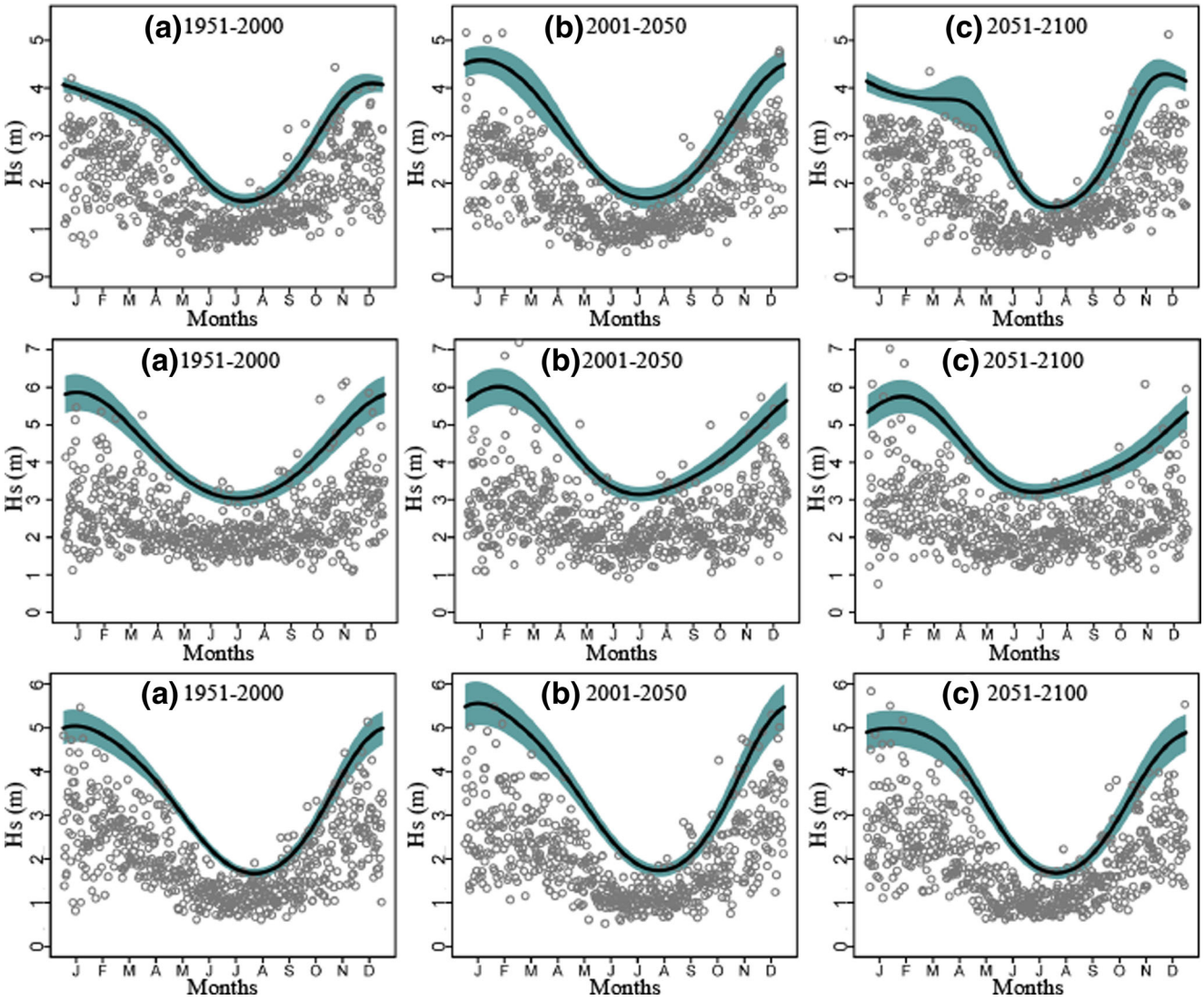

Fig. 14 Ninety-eight percent significant wave height (H_s) quantiles within a year for the marine areas of Alexandroupoli, Heraklion and Kyparissia, from *top* to *lower graphs*. Panels correspond to **a** reference, **b** current and **c** future periods, from *left* to *right*

increases are observed for the upper 95 % confidence limits of the return level estimates. However, for the future period a decrease in extreme wave heights is evident, compared to those of the current period, especially for events with a high probability of occurrence. For a return period of 50 years, the extreme wave heights in the future period are more than 10 % higher compared to the respective estimate for the reference period. Moreover, the uncertainty represented by the range of the return level confidence interval also appears higher for the future period. In the marine area of Heraklion, climate change effects on extreme wave heights are not obvious. Extreme wave heights are almost stable for the current and reference periods estimates, whereas a slight decrease in extreme H_s can be noticed for the future period. In the marine area of Kyparissia, increases in extreme H_s of the current period are evident (exceeding 14 % for 50-year return period). H_s extremes appear reduced in the future period compared to those of the first half of the twenty-first century, but still higher (over 6 % for 50-year return period) than the respective ones of the reference period.

4.3 Analysis of storm surge intra- and inter-annual extremes

The results of GreCSSM are presented and discussed concerning the evolution of extreme sea levels due to storm surges from 1951 to 2100. Indicative intercomparisons of results (*SSI*, annual *SLH* maxima and inter-annual extremes) for three 50-year periods are provided.

4.3.1 Regional analysis

The present and future, intra- and inter-annual variability of *SLH* maxima in the entire Mediterranean Sea (level I) was

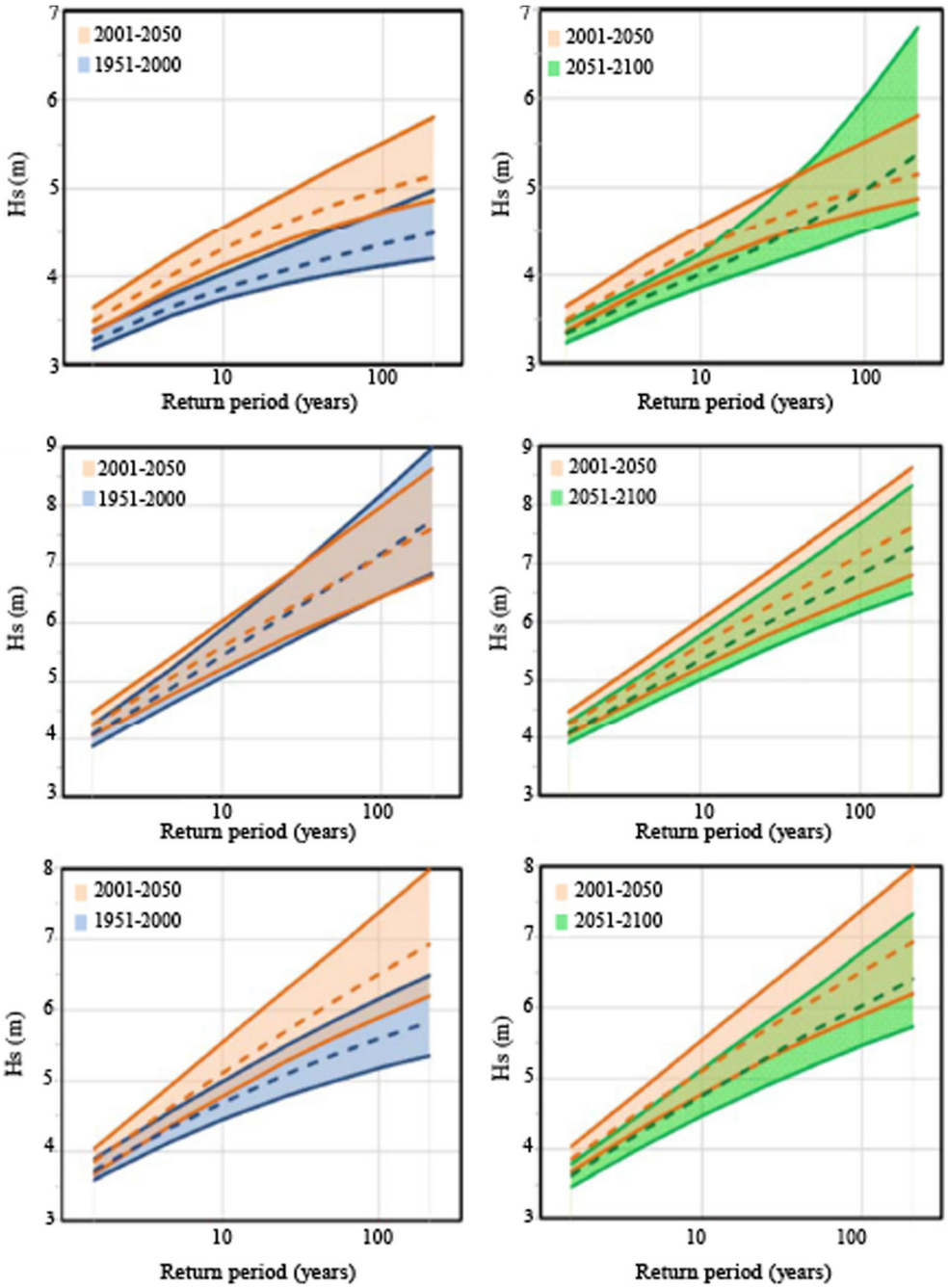

Fig. 15 Annual return levels of significant wave height (H_s) for the marine areas of Alexandroupoli, Heraklion and Kyparissia, from *top* to *lower graphs*. Comparisons of the reference period (1951–2000) against the current period (2001–2050) and the current against the future period (2051–2100) are given in the *left* and *right graphs*, respectively. *Dashed lines* correspond to *MLEs* and *solid lines* to the upper and lower 95 % confidence bounds

investigated by Androulidakis et al. (2015). The *SLH* maxima were estimated to increase during 2001–2050 compared to those during the reference period. This increase is expected to relax in the future period. Their results also indicate that the maximum surges increase by almost 3.5 % in the current period, compared to those of the reference period, whereas they are estimated to decrease by an average of 7 % for 2051–2100 compared to those of 2001–2050 over the entire Mediterranean Sea. The projected attenuation of storminess over the eastern Mediterranean basin under the SRES-A1B scenario, also suggested by other researchers (Conte and Lionello 2013, Marcos et al. 2011), was reflected in their results with a reduction of average storm-induced sea level (SLH_{mean}) throughout the twenty-first century (of the order of 17 % and 5 % for the current and future periods, respectively).

Based on the results of the GreCSSM simulations (level II), Fig. 16 shows the corresponding horizontal distributions of maximum and average (upper and lower graphs, respectively) *SLH* for the three periods. In general a significant increase of *SLH* maxima is estimated for the first half of the twenty-first century, compared to those of the reference and the future

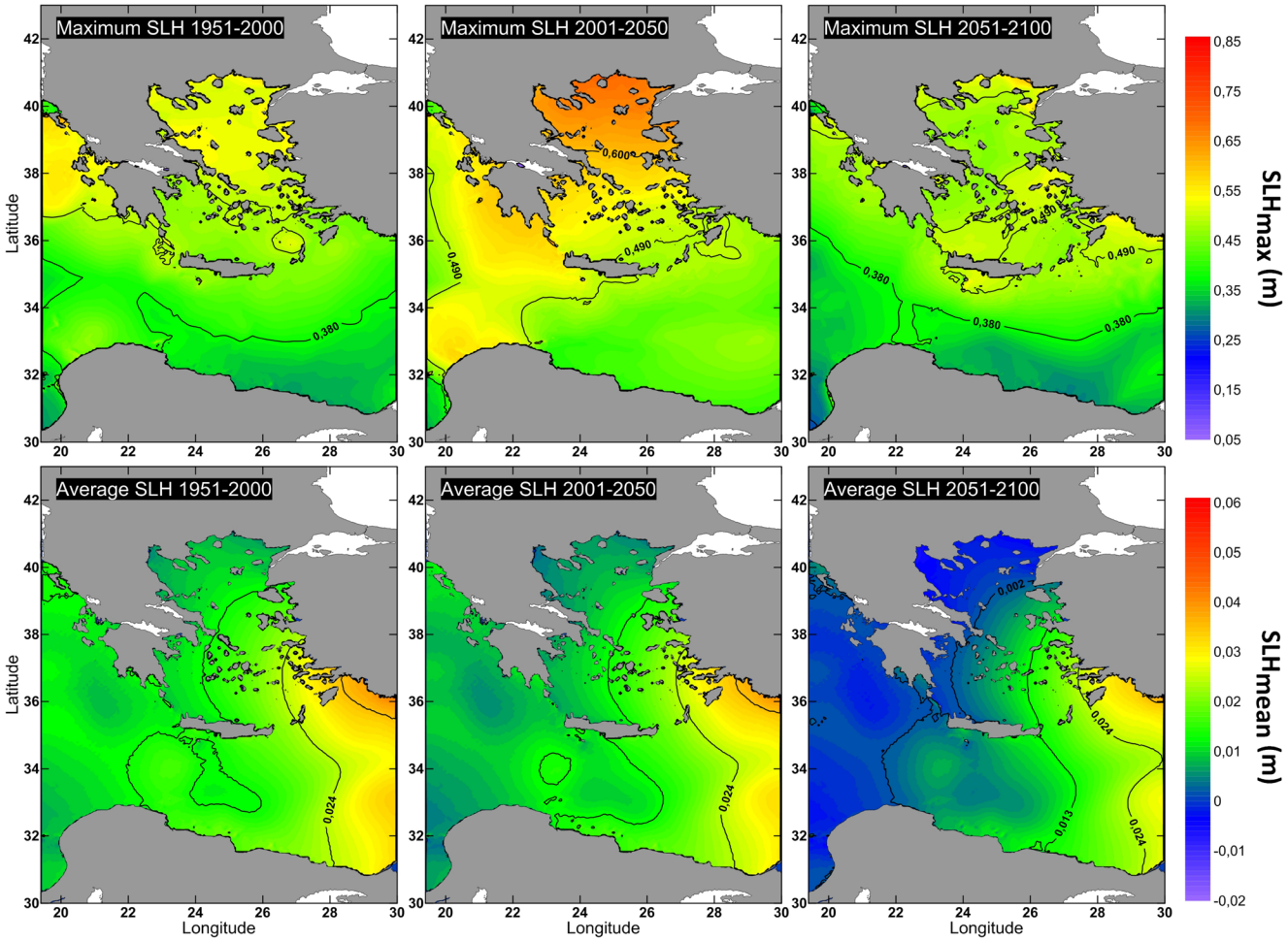

Fig. 16 Horizontal distribution of maximum (*upper graphs*) and average (*lower graphs*) *SLH* (m) in the study area for the reference (1951–2000), current (2001–2050) and future (2051–2100) periods (from *left* to *right*)

periods. Magnitudes range between 0.60 and 0.85 m in the North Aegean Sea with higher values along the northern coasts, while the corresponding values for the reference period are of the order of 0.50–0.55 m. In the southern AIS, *SLH* maxima are estimated to range between 0.50 and 0.60 m in 2001–2050, whereas the values of the reference period are found to be almost 10 cm lower. Towards the end of the twenty-first century, the peak *SLH* values reduce significantly in most parts of the study area, ranging from 0.50 to 0.60 m in the North Aegean Sea and from 0.40 to 0.50 m in the Ionian Sea. Surge maxima are estimated to remain similar to the levels of the current period over the northeastern part of the South Aegean and western Crete. Moreover, an attenuation of storminess and related surge maxima is expected for the AIS during 2051–2100. Nevertheless, the magnitude of extreme surges is expected to increase during the first half of the twenty-first century (30 ~ 40 % in North Aegean). The spatiotemporal variability of average surge-induced sea level (Fig. 16, lower graphs) reveals that there is a stable pattern of SLH_{mean} with increasing values from West to East. Although there are no distinct differences between the reference and the current period, a strong decrease of SLH_{mean} values can be observed for the second half of the twenty-first century.

The representative annual maxima of *SLH* that may occur for the current and future periods can be described by *SSI* (Section 3.3). Figure 17 presents the averaged (for each of the three periods) values of annual *SSIs* over each 50-year period ($SSI_{50\text{-yr}}$). The graphs refer to the spatial variability of $SSI_{50\text{-year.}}$ along the coastal zone of the study area, including the entire Greek coastline and the coasts of Anatolia and North Africa that surround the Aegean and Libyan Seas, respectively. The spatial distribution pattern of $SSI_{50\text{-yr.}}$ is similar to that of annual *SLH* maxima in the preceding discussion for each particular coastal region investigated. The highest *SSI* values (>0.4 m) can be traced along the northern coasts of the Aegean Sea (coastal zone of Alexandroupoli). Values decrease from North to South, ranging from 0.32 to 0.38 m for the central parts of the AIS, falling to almost 0.3 m in the southern part of the AIS (South Aegean and Crete), and below 0.25 m for the northern African coasts. The temporal evolution of $SSI_{50\text{-year}}$ values shows significant regional differences mostly in the 2051–2100 period; lower values occur along the entire

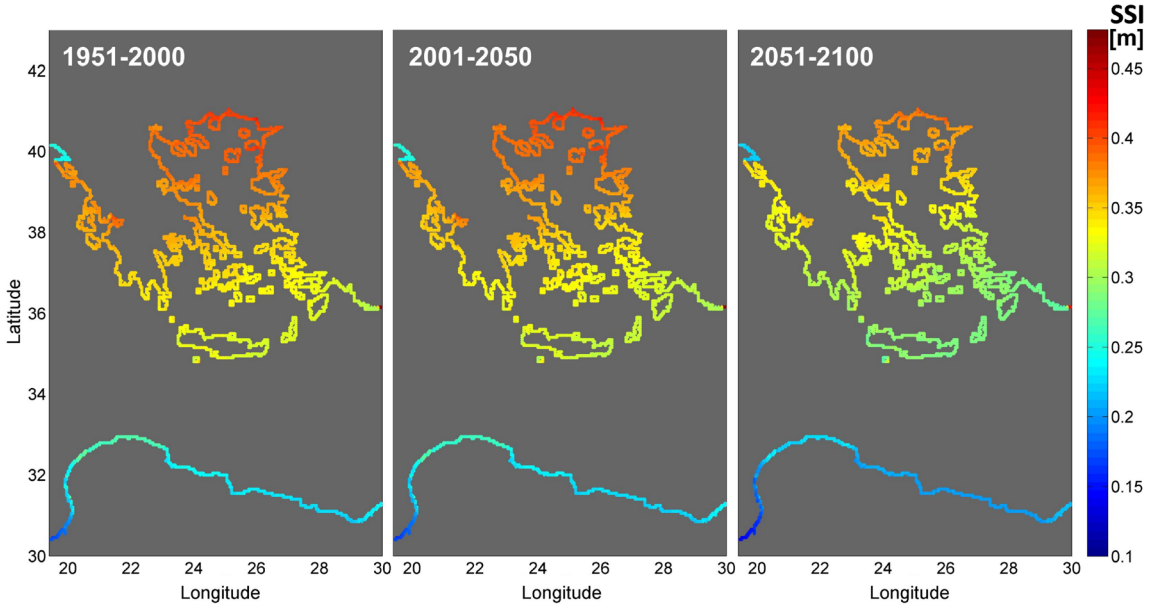

Fig. 17 Storm Surge Index *SSI* (m) along the coastline of the study area, time-averaged over the 50-year reference, current and future periods (from *left* to *right*)

coastline, consistent with the estimated storm attenuation during the future period. The change in $SSI_{50\text{-year}}$ between the first half of the twenty-first century and the reference period are generally low, ranging from −1.4 to +0.8 cm (differences of −5.1 % to +19.6 %) with an average value of −0.6 cm (1.6 % decrease). Storm surge events may be more infrequent in the current period resulting to averaged $SSI_{50\text{-yr.}}$ values of similar levels with those of the reference period, yet higher surge maxima may occur during 2001–2050 (Fig. 16). *SSIs* generally decrease from the current to the future period, with differences between −4.7 and 0.02 cm (changes of −17.5 % to +1.8 %) and a − 2.6 cm average *SLH* (8 % decrease).

Figure 18 presents the average duration in hours (red curves) and the average number of grid cells (blue curves), i.e. the spatial coverage, of storm surge events with *SLH* values exceeding the severe event threshold. The latter is defined statistically by $(m + 3\sigma)_{SLH,obs} \approx 30$ cm based on in situ measurements at five Greek stations for an 18-year period (see also Section 3.3); Fig. 18 graphs refer to each of the main subregions of the study area (Fig. 2c). By setting the confidence level at 95 % (p values <5 %) for the Mann-Kendall test, only the statistically significant monotonic trends are indicated with straight lines for each parameter, separating the reference period from the twenty-first century; values of the corresponding linear trend slopes are also noted on the graphs. The maximum values of storm surges' spatial coverage are observed in the central part of the Aegean Sea, while the most frequent high-duration surges over the severe event threshold are estimated to occur in the Ionian Sea. During the reference period no distinctive trend is observed, both in terms of duration and coverage in all regional seas, apart from the North Aegean, where a strong decrease in both factors can be noticed. In contrast, both parameters decrease for the SRES-A1B-based run throughout almost the entire domain. The only exception is the North Aegean region, where no statistically significant trend (based on the Mann-Kendall test) exists for the spatial coverage of storm surges. This decreasing tendency is in agreement with the projected storminess attenuation. However, even though the general future trends decrease, short-term peaks are observed in the time series that exceed the values of the past climate. For example, the total annual duration of storms in the southwestern part of the study domain (e.g. the Ionian Sea) shows maxima that are higher than the respective ones of the reference period, especially in the current period; the corresponding maximum spatial coverage values remain at similar levels. On the other hand, in the South Aegean the largest peaks in spatial coverage are estimated to occur during 2001–2050, marginally exceeding the ones of the reference climate. In the North Aegean Sea, the values of storm surges' spatial coverage generally fluctuate over the same range in the entire twenty-first century. Future trends in both the spatial coverage and the duration of storm surges are generally estimated to decrease. Nevertheless there is a high possibility of short-term surge events with higher duration and/or coverage in parts of the domain, especially in 2001–2050.

The occurrence frequency of annual SLH_{max} per season is also calculated at all stations for the three 50-year periods, in order to investigate potential changes in the seasonal variability of annual storm surge maxima. As expected, most of the large events take place during winter and spring for all stations. The simulation output shows a decrease of winter frequencies in the second part of the twenty-first century, along with a corresponding increase of spring values, throughout almost the entire AIS region. No summer storm surge maxima are reproduced in any of the study periods. Therefore,

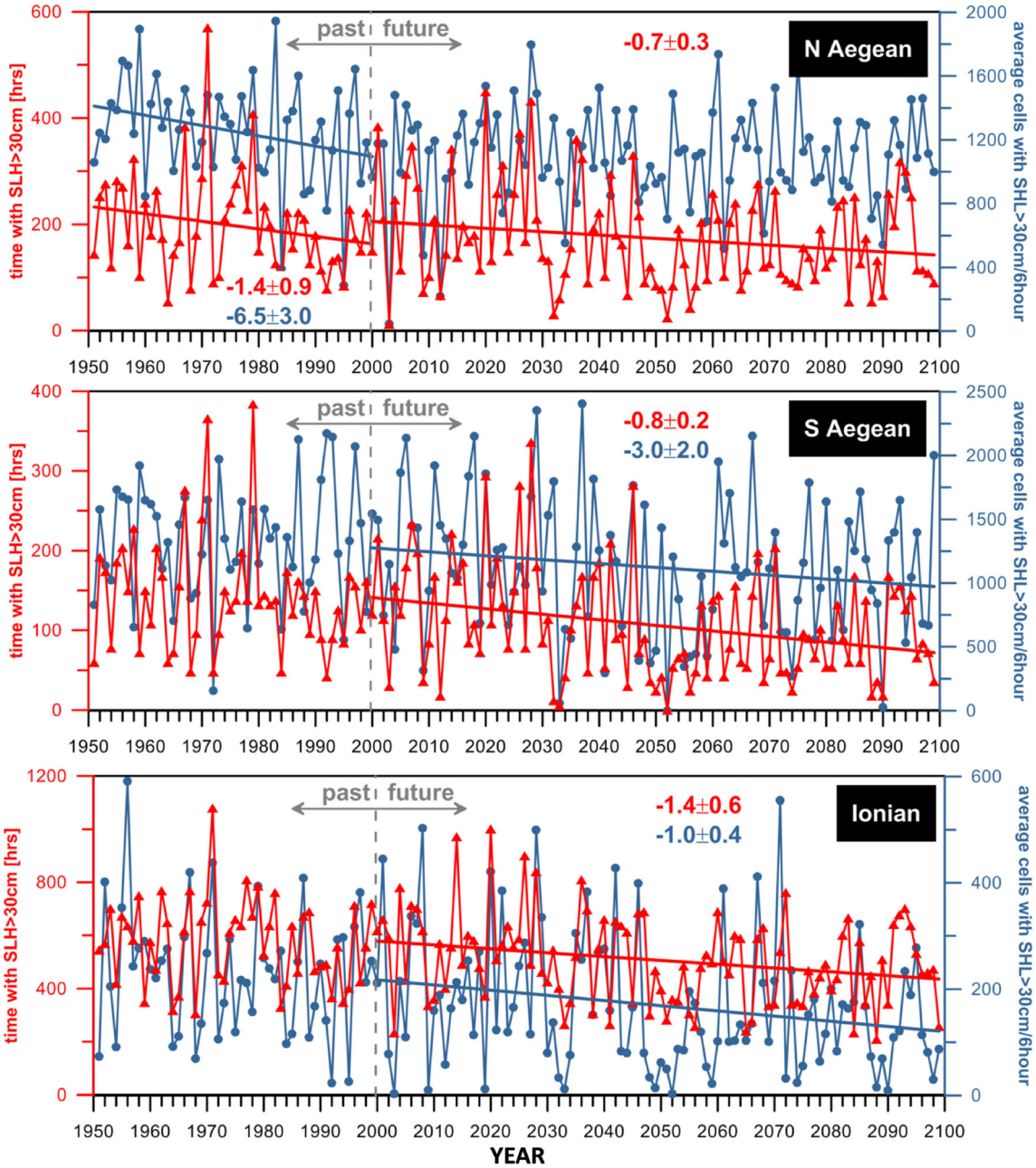

Fig. 18 Annual duration (h) (*red curve with triangles*) and corresponding average number of model cells (*blue curve with dots*) with $SLH > (m + 3\sigma)_{SLH,obs} \approx 30$ cm for the main subregions of the AIS (see Fig. 2e). Linear trends with 95 % confidence level (*straight lines*) for each parameter, divided in the reference period and the entire twenty-first century; values of trend slopes noted on the plots with corresponding colour

modelling results show a general increase in the range of the seasonal cycle of storm surges, with a decrease of winter-autumn and an increase of spring frequencies. These findings are in agreement with Jordà et al. (2012).

4.3.2 Analysis of extreme storm surges

A similar approach used for the wave height extremes (Section 4.2.2) is utilized for the storm surge monthly maxima. The best-fit nonstationary GEV models, describing the variability of monthly extremes for storm surge events, present fewer differences in their structure among the selected areas of the AIS, compared to the ones used for the wave height extremes. Especially for the future period, GEV distribution functions have one harmonic in their location parameter (μ), two harmonics in their scale parameter (σ) and a constant shape (ξ), in almost all study areas. For the reference period an annual cycle (single harmonic) is evident in the

location and shape parameters, whereas both the annual and seasonal cycles are considered statistically significant (based on the deviance statistic D) for the scale parameter. The shape parameter of the GEV is kept constant only for the areas in the South Aegean Sea (Heraklion and Chania). For the current period the dominant models in the North Aegean Sea (Alexandroupoli, Katerini and Lesvos) are characterized by two harmonics in the parameters μ and σ and by one harmonic in ξ. For the same period in the South Aegean Sea, the seasonal cycle in ξ is also considered statistically significant (based on D). In the Ionian Sea some differences are found in the best-fit models of the three areas of focus (Parga, Kyparissia and Kerkira), mainly detected in the number of harmonics in ξ.

Figure 19 presents the 98 % storm surge quantile levels corresponding to a return period of 50 years within a stationary context in a yearly time interval for all three periods considered in the marine areas of Alexandroupoli, Heraklion and Kyparissia. *MLEs* of quantiles are represented with a solid line and the shaded areas correspond to the 95 % confidence intervals estimated using the delta method. The monthly maxima of each sample in chronological order are also included as points. A peak of the 98 % storm surge quantile is observed in December for the reference period in all three study areas of the North Aegean Sea. Extreme storm surges decrease quite slowly during winter and until the end of spring. For the same period in the study areas of the South Aegean and the Ionian Sea, the peak of the extreme storm surges appears within and at the end of winter, respectively. Storm surge extremes present mild changes during the entire winter period until mid-spring. During the current period, the peak of the extreme storm surges in the study areas of the North Aegean Sea is

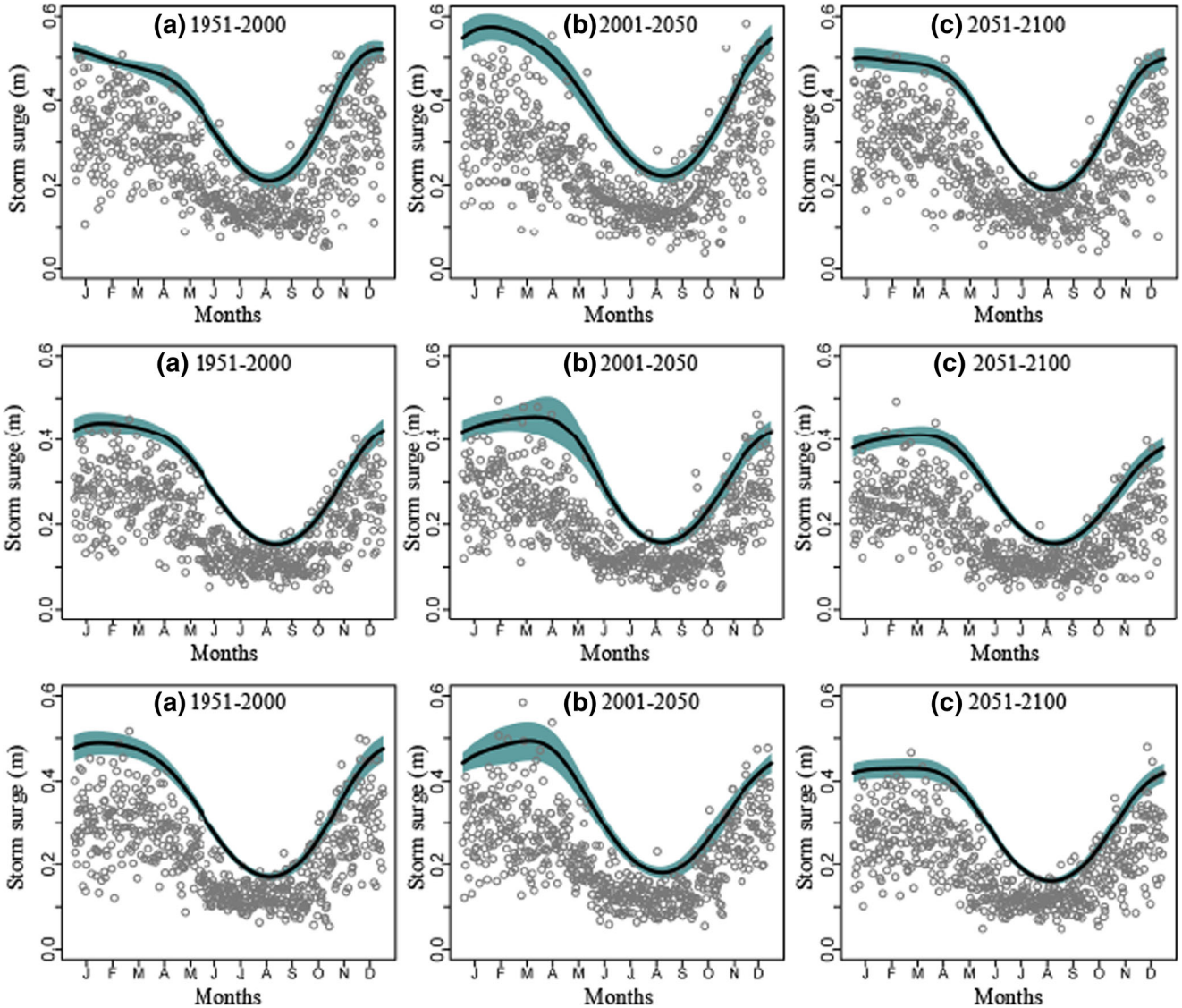

Fig. 19 Ninety-eight percent storm surge (*SLH*) quantiles within a year for the marine areas of Alexandroupoli, Heraklion and Kyparissia, from *top* to *lower graphs*. Panels correspond to **a** reference, **b** current and **c** future periods (from *left* to *right*)

observed at the end of winter and is more prominent compared to the other periods. In the South Aegean Sea and in most of the study areas in the Ionian Sea, the peak of the extreme storm surge quantile appears in mid-spring. Especially for the marine areas of Heraklion and Chania (South Aegean Sea), the uncertainty of the peak storm surge quantiles in this interval is significantly increased. For the future period, the study areas in the North Aegean and the Ionian Sea present similar characteristics. There is a quite elongated time span that covers the period of peak values and extends up to the first spring months, where the storm surge quantile variation is insignificant. On the other hand, in the study areas of the South Aegean Sea the peak of the extreme storm surge quantile in the future period appears in mid-spring, but the uncertainty that accompanies these estimates is significantly reduced.

Figure 20 presents annual storm surge return levels of return periods between 2 and 200 years in the marine areas of Alexandroupoli, Heraklion and Kyparissia for the three 50-year periods shown in successive pairs

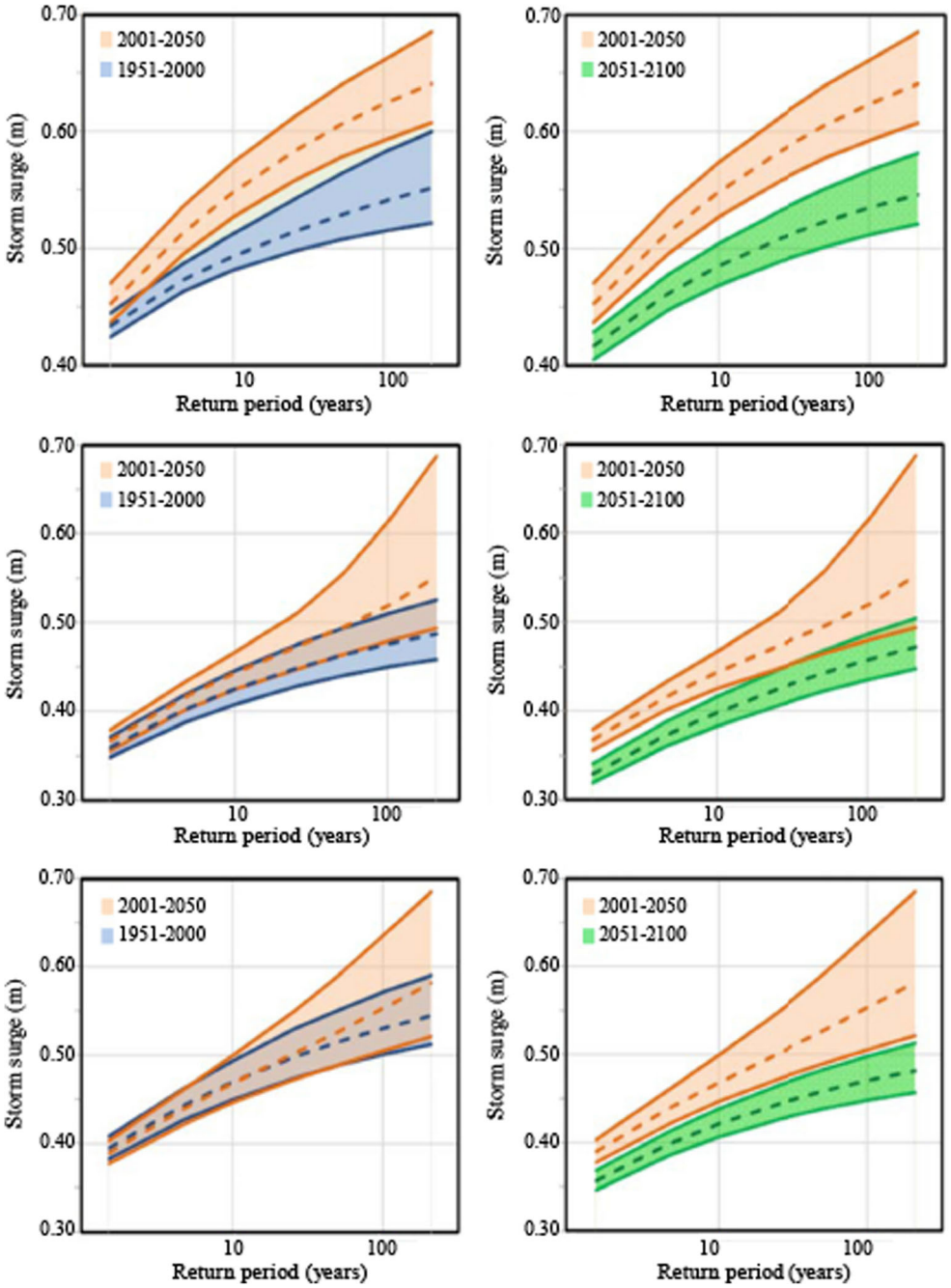

Fig. 20 Annual return levels of storm surges (*SLH*) for the marine areas of Alexandroupoli, Heraklion and Kyparissia, from *top* to *lower graphs*. Comparisons of the reference (1951–2000) against the current (2001–2050) period and the current against the future (2051–2100) period are given in the *left* and *right graphs*, respectively. *Dashed lines* correspond to *MLEs* and *solid lines* to the upper and lower 95 % confidence bounds

(1951–2000 with 2001–2050, 2001–2050 with 2051–2100). It is evident that there is an increase in extreme storm surges in the marine area of Alexandroupoli for the current period with respect to those of the reference period. This increase in storm surge *MLEs* is estimated at almost 15 % for a return period of 50 years. For the future period, there is a decrease of the extreme storm surges in the area, compared to those of the current period, exceeding 13.5 % for a return period of 50 years. Therefore, the *SLH* return level estimates for 2051–2100 are close to the ones extracted for the reference period. These findings are in agreement with the discussion in Section 4.3.1, regarding annual *SLH* maxima. In the marine area of Heraklion extreme storm surges present an increase in the current period, compared to those of the reference period, reaching almost 7 % for a return period of 50 years. The range of the 95 % confidence interval is almost doubled (the extreme value distribution fitted to *SLH* extremes belongs to the domain of attraction of a Fréchet distribution), compared to the respective estimates for the reference period (the extreme value distribution fitted to *SLH* extremes belongs to the domain of attraction of a Weibull distribution), significantly raising the return level uncertainty. Storm surge return level estimates and confidence intervals are significantly reduced in the future period. In the marine area of Kyparissia, there is stability in *MLEs* of extreme storm surges for the reference and the current period. Slight increases can be observed for the latter only for sufficiently high return periods; thus, the following results correspond to analysis based on a 50-year return period. The range of the 95 % confidence interval for the current period appears increased by almost 65 % (the extreme value distribution fitted to *SLH* extremes belongs to the domain of attraction of a Fréchet distribution), compared to the respective estimate for the reference period (the extreme value distribution fitted to *SLH* extremes belongs to the domain of attraction of a Weibull distribution). During the future period, there is a decrease of extreme storm surges reaching 13 % for a 50-year return period compared to the other two periods.

4.4 Climate change signals

In order to gain a more general insight on the climate change signals of the storm-induced sea-surface dynamics in the AIS during the twenty-first century, we use the Climate Change Index (*CCI*). *CCI* is calculated on the coastal zone concerning the storm surges, and over entire subregions of the AIS concerning the wave fields. For example the *CCI* of intra-annual storm surge maxima *SSI* on every coastal cell of the AIS numerical domain and through each of the current and future 50-year periods in reference to 1951–2000 is given by

$$CCI_{SSI,Future}\,(\%) = 100\cdot\frac{\left(\overline{SSI_{mod}^{(Future\ Period)}} - \overline{SSI_{mod}^{(Reference\ Period)}}\right)}{\left(\overline{SSI_{mod}^{(Reference\ Period)}}\right)}$$

$$CCI_{SSI,Current}\,(\%) = 100\cdot\frac{\left(\overline{SSI_{mod}^{(Current\ Period)}} - \overline{SSI_{mod}^{(Reference\ Period)}}\right)}{\left(\overline{SSI_{mod}^{(Reference\ Period)}}\right)} \quad (2)$$

where the overbar denotes temporal (50-year) averages of *SSI* calculated along the coastal zone of the main subregions (Fig. 2c) of the AIS. *CCI* is then spatially averaged over all of the subregion's nearshore marine cells. The $m \pm \sigma$ (σ of *CCI* values is the standard deviation in spatial terms) values of $CCI_{SSI,current}$ are −2.48 ± 1.24 %, −0.65 ± 0.93 % and −2.09 ± 0.47 %, for the Ionian, North and South Aegean, respectively. These values reveal a general small decrease of storm surge annual maxima with a miniscule possible increase only in the North Aegean for the current period (2001–2050). The respective $m \pm \sigma$ values of $CCI_{SSI,future}$ are −10.11 ± 1.08 %, −7.17 ± 1.46 % and −9.94 ± 1.02 %. Thus, a general clear attenuation of storm surge annual maxima is expected on the entire coastal zone of the AIS for the second half of the twenty-first century. This is qualitatively consistent with the findings of Marcos et al. (2011), Jordà et al. (2012), Lionello et al. (2012), Šepić et al. (2012), Conte and Lionello (2013), Androulidakis et al. (2015).

CCI is also calculated for the annual maxima of SWH, $H_{s,max}$ (*SSI* replaced by $H_{s,max}$ in Eq. 2). The $m \pm \sigma$ values of $CCI_{Hs,max,current}$ are 3.83 ± 1.91 %, 3.85 ± 1.69 % and 1.57 ± 2.10 %, for the Ionian, North and South Aegean, respectively. These values reveal a general small increase of SWH annual maxima with a minor possible decrease only in the South Aegean for the current period (2001–2050). The respective $m \pm \sigma$ values of $CCI_{Hs,max,future}$ are 2.06 ± 2.49 %, 0.45 ± 2.04 % and 0.21 ± 3.27 %; thus, a general attenuation of spatially averaged $H_{s,max}$ is expected in the AIS during the second half of the twenty-first century compared to the current period. This is in accordance to the deductions of Lionello et al. (2008, 2012), Benetazzo et al. (2012), Casas-Prat and Sierra (2013). Note that *CCI* concerning $T_{-10,max}$ (annual maximum T_{-10}) is also under a decreasing trend throughout the twenty-first century in comparison to the reference period, but changes are smaller than the ones of H_s fields. They are practically negligible specifically in the Aegean Sea, which is generally reasonable, since fetch-limited seas prevail there. Further analysis of mean and extreme wave directionality

should shed more light about the magnitudes of extreme wave lengths and periods in future studies.

All the above signify a clear pattern of marine (and consequently atmospheric) climate change signals in the AIS during the twenty-first century, which is characterized by a general attenuation trend of the storm severity and a consequent generic debilitation of severe marine events towards the end of the twenty-first century. The most probable cause for that is the weakening of winds and cyclonic activity over the Mediterranean towards 2100 (Marcos et al. 2011), and the consequent negative future trend of the mean storm-induced *SLH* (Jordà et al. 2012). Thus, we have also deduced that single severe events could be of increased strength, yet they would more infrequent (Marcos et al. 2011). Seasonality of extreme marine events (e.g. reduction of winter SLH_{max}) could be linked to the number and intensity of cyclones reported by Jordà et al. (2012); i.e. the positive trend of the NAO index especially in winter and the poleward shift of storm tracks, could be the main reasons for the projected higher *SLP* values specifically in the AIS (Šepić et al. 2012). This is consistent with the decrease of extreme *SLH* towards 2100 found in the present study. Moreover surges are mainly induced by winds in coastal areas of wide and shallow continental shelfs, but that is hardly the case in the AIS. *SLPs* are better represented in our analysis compared to winds; therefore, the presented estimations of storm surge events should be adequately reliable. Ultimate scope of the study is to avoid overestimations of flood risks along Greek coastal areas in the future. Wind-driven waves are found to probably follow a decreasing trend in the AIS (east-central Mediterranean) during the twenty-first century attending the general pattern of milder marine storm extremes in the future period than the reference one (also derived by Lionello et al. 2008), with minor exceptions during summertime in most of the study areas (also found by Benetazzo et al. 2012).

5 Conclusions

In this paper changes in the wind, *SLP*, wave and storm surge characteristics of the Aegean and Ionian Seas (AIS) under the SRES-A1B emission scenario are investigated for the first and the second half of the twenty-first century in comparison with a reference period (1951–2000).

The analysis of simulated wind patterns over Greece shows that the (mainly north and northeastern) wind direction is estimated to remain invariant throughout the twenty-first century in the Aegean Sea. This means that the prevailing synoptic systems over the Balkan Peninsula and eastern Mediterranean, which mainly form and affect wind directions, are expected to remain generally stable as far as their centre locations are concerned. The estimated reinforcement of the Etesian winds during the summer period in the future is attributed to the deepening of the Asian thermal low and the West Africa heat low.

The assessment of climate change (based on SRES-A1B) effects on the sea-surface dynamics of the AIS until the end of the twenty-first century entails two main signals for the simulated mean wave fields (based on H_s), while a distinct signal of general attenuation is estimated for the storm surges. Specifically, the mean SWH fields in the AIS are estimated to follow the general storminess attenuation from the reference to the future period. The same pattern applies to the annual maxima SWH fields of the Ionian, Libyan and Levantine Seas, while a persistent increase of yearly peaks is expected in the central and northern Aegean Sea. The southern Aegean Sea is mildly affected by these changes due to the limited flow through the two Cretan straits. The second signal is associated with the increase of Etesian winds, which are expected to significantly affect the central, south and southeastern Aegean wave climate, especially during summer and autumn. In contrast with the general trend, increased wave energy is observed during the low-energy season, particularly to those regions of the Aegean with large northerly fetches, i.e. north of Cyclades island group and Crete. In accordance to the findings of Conte and Lionello (2013), the storm surge simulations also show a clear attenuation of storminess and inter-annual surge maxima for the AIS, especially during the future period. Magnitudes of annual surge maxima are expected to increase by 30–40 % in the North Aegean during the current period, while their frequency of occurrence is estimated to decline. The attenuation signal is also related to the generally decreasing spatiotemporal trends of storm surges under SRES-A1B scenario. Storm surges are estimated to intensify in the North Aegean Sea, especially in the first half of the twenty-first century, unlike the South Aegean Sea where they will probably debilitate. Nevertheless, storm surges in the coastal zones of northern Greece are expected to remain stably larger than in the southern parts of the country in the twenty-first century, rendering the North Aegean low-land coastal areas more prone to flooding than others in the AIS. The general attenuation patterns are due to changes in the seasonal variability of atmospheric patterns and barometric centres. An estimated expansion of the annual cycle of storm surges towards the warmer period of the year is shown throughout the entire domain, consistent with Jordà et al. (2012).

The analysis of extreme wave heights in the North Aegean Sea reveals a significant increase in their severity during the current period, as well as a pronounced increase in prediction uncertainty during the future period, especially for high return periods (compared to the reference period). In the South Aegean, there are no evident climate change effects on extreme wave heights. In the Ionian Sea, extreme wave heights are expected to increase during the current period, while return level estimates close to those of the reference period are estimated for the future period. Extreme storm surges are also

estimated to increase in the North and South Aegean Sea (current period), while return level values close to those of the reference period have been estimated for the future period. In the Ionian Sea, there is a relative stability in the *MLEs* of extreme storm surges for the reference and the current period, while a significant increase in prediction uncertainty is evident in the latter. During the second half of the twenty-first century storm surge extremes are estimated to be lower than those of the reference period. The findings for the *SLP* changes during winter show an increase of surface pressure for both the current and the future period, while even though wind speeds are generally estimated to increase in the AIS during the current period, they may decrease in the last 50 years of the twenty-first century. Thus, it seems that the extreme storm surges are mainly affected by the changes in wind speeds rather than changes in the synoptic conditions over the domain of study. In general, there is an indication of a seasonal time shift from winter to spring in the occurrence of the most extreme storm surges in the AIS between the reference and current period.

All things considered, our results imply a specific mechanism of regional climate change, i.e. we identify an expected self-regulating behaviour of the marine and atmospheric climate in the Mediterranean region and specifically in the AIS. We estimate a projected intensification of severe events during the first half of the twenty-first century under the SRES-A1B scenario and subsequent storminess attenuation towards the end of the twenty-first century; this leads to resettlement of milder extreme marine events, but of significantly higher uncertainty. Nonetheless, even though the dynamically downscaled implementation of the specific RCM used provided satisfactory results in comparison to reanalysis data used as evaluation standards, extra attention should always be given to its physical parameterizations, the orography and size of the model domain, the forcing input (emission scenarios, etc.) and the assimilation of large-scale meteorological forcing (Giorgi and Mearns 1991, 1999). Giorgi and Anyah (2012) mention that RegCM's hydrostatic nature induces some limitations, when it is applied on very high-resolution domains. Their long-term goal is to provide a fully coupled regional Earth System Model with other components of the climate system aiming on even better simulations of the present climate and furthermore reliable future scenarios.

The literature review for the expected MSL from various scenarios shows relatively small *SLR* in the Mediterranean due to the steric effect of about 10 cm for the current period and 30 cm for the future period. However, these results strongly depend on the Atlantic dataset used to force the regional models at the boundary with the open ocean (Slangen et al. 2016). Similarly, but at regional scale, results may depend on the Black Sea forcing of the Aegean Sea. The mass addition will contribute a supplementary and approximately equal amount to the *SLR* (i.e. of about 10 cm for the current and 30 cm for the future period), provided that the recently measured trends remain the same until the end of the twenty-first century.

Future research should focus on the estimation of climate change impacts on coastal vulnerability of the AIS taking into account the combined effects of extreme waves and storm surges, superimposed on the projected *MSL* rise. This kind of assessment is crucial for twenty-first century coastal policies in the AIS, regarding the design levels of protection measures.

Acknowledgments This research has been co-financed by the European Union (European Social Fund—ESF) and Greek national funds through the Operational Program "Education and Lifelong Learning" of the National Strategic Reference Framework (NSRF)—Research Funding Program: Thales. Investing in knowledge society through the European Social Fund (Project CCSEAWAVS: Estimating the effects of Climate change on SEA level and WAve climate of the Greek seas, coastal Vulnerability and Safety of coastal and marine structures). The tide-gauge data of sea level variations, used for the validation of the storm surge model, were provided from the HNHS (http://www.hnhs.gr/portal/page/portal/HNHS). Satellite altimetry data were obtained from AVISO (http://www.aviso.oceanobs.com/).

References

Adloff F, Somot S, Sevault F, Jordà G, Aznar R, Deque M, Herrmann M, Marcos M, Dubois C, Padorno E, Alvarez-Fanjul E, Gomis D (2015) Mediterranean Sea response to climate change in an ensemble of twenty first century scenarios. Clim Dyn 45:2775–2802

Anagnostopoulou C, Zanis P, Katragkou E, Tegoulias I, Tolika K (2014) Recent past and future patterns of the Etesian winds based on regional scale climate model simulations. Clim Dyn 42:1819–1836

Androulidakis YS, Kombiadou KD, Makris CV, Baltikas VN, Krestenitis YN (2015) Storm surges in the Mediterranean Sea: variability and trends under future climatic conditions. Dynam Atmos Ocean 71: 56–82

Athanassoulis GA, Belibassakis KA (2002) Probabilistic description of metocean parameters by means of kernel density models 1. Theoretical background and first results. Appl Ocean Res 24(1):1–20

Athanassoulis GA, Skarsoulis EK (1992) Wind and wave atlas of the northeastern Mediterranean Sea. Loukakis TA (ed), Laboratory of Ship and Marine Hydrodynamics, Dept. of Naval Architecture and Marine Engineering, National Technical University of Athens, Greece. Prepared under the authority of Hellenic Navy General Staff

Athanassoulis GA et al (2004) Wind and wave atlas of the Mediterranean Sea. Western European Armaments Organisation Research Cell

Barry RG, Carleton AM (2001) Synoptic and dynamic climatology. Routledge: Taylor and Francis, London

Becker JJ, Sandwell DT, Smith WHF, Braud J, Binder B, Depner J, Fabre D, Factor J, Ingalls S, Kim S-H, Ladner R, Marks K, Nelson S, Pharaoh A, Trimmer R, Von Rosenberg J, Wallace G, Weatherall P (2009) Global bathymetry and elevation data at 30 arc seconds resolution: SRTM30_PLUS. Mar Geod 32(4):355–371

Benetazzo A, Fedele F, Carniel S, Ricchi A, Bucchignani E, Sclavo M (2012) Wave climate of the Adriatic Sea: a future scenario simulation. Nat Hazards Earth Syst Sci 12:2065–2076

Berrisford P, et al. (2011) The ERA-Interim archive [Version 2.0]. European Centre for Medium Range Weather Forecasts, Shinfield Park. Reading, Berkshire RG2 9AX, UK

Booij N, Ris RC, Holthuijsen LH (1999) A third-generation wave model for coastal regions: 1. Model description and validation. J Geophys Res Oceans (1978–2012) 104(C4):7649–7666

Carillo A, Sannino G, Artale V, Ruti PM, Calmanti S, Dell'Aquila A (2012) Steric sea level rise over the Mediterranean Sea: present climate and scenario simulations. Clim Dyn 39(9–10):2167–2184

Casas-Prat M, Sierra JP (2013) Projected future wave climate in the NW Mediterranean Sea. J Geophys Res Oceans 118:3548–3568

Charles E, Idier D, Delecluse P, Déqué M, Cozannet G (2012) Climate change impact on waves in the Bay of Biscay, France. Ocean Dyn 62:831–848. doi:10.1007/s10236-012-0534-8

Christopoulos S (1997) Wind-wave modelling aspects within complicate topography. Ann Geophys 15(10):1340–1353

Coles S (2001) An introduction to statistical modelling of extreme values. Springer, London, p. 209

Conte D, Lionello P (2013) Characteristics of large positive and negative surges in the Mediterranean Sea and their attenuation in future climate scenarios. Glob Planet Change 111:159–173

Cox DT, Kobayashi N (2000) Identification of intense, intermittent coherent motions under shoaling and breaking waves. J Geophys Res Oceans (1978–2012) 105(C6):14223–14236

De Vries H, Breton M, de Mulder T, Krestenitis Y et al (1995) A comparison of 2D storm surge models applied to three shallow European seas. Environ Softw 10(1):23–42

De Winter RC, Sterl A, de Vries JW, Weber SL, Ruessink G (2012) The effect of climate change on extreme waves in front of the Dutch coast. Ocean Dynam 62(8):1139–1152

Dee DP et al (2011) The ERA-Interim reanalysis: configuration and performance of the data assimilation system. Q J R Meteorol Soc 137(656):553–597

Dykes JD, Wang DW, Book JW (2009) An evaluation of a high-resolution operational wave forecasting system in the Adriatic Sea. J Marine Syst 78:S255–S271

Emanuel KA (1991) A scheme for representing cumulus convection in large-scale models. J Atmos Sci 48(21):2313–2335

Esteves LS, Williams JJ, Brown JM (2011) Looking for evidence of climate change impacts in the eastern Irish Sea. Nat Hazards Earth Syst Sci 11:1641–1656

Fritsch JM, Chappell CF (1980) Numerical prediction of convectively driven mesoscale pressure systems. Part II. Mesoscale model. J Atmos Sci 37:1734–1762

Galanis G et al (2012) Wave height characteristics in the Mediterranean Sea by means of numerical modelling, satellite data, statistical and geometrical techniques. Mar Geophys Res 33(1):1–15

Gil VE, Genovés A, Picornell MA, Jansà A (2002) Automated database of cyclones from the ECMWF model: preliminary comparison between west and east Mediterranean basins. *Proc 4th EGS Plinius Conference*, Mallorca, Spain

Giorgi F, Anyah RO (2012) The road towards RegCM4. Clim Res 52:3–6

Giorgi F, Mearns LO (1999) Introduction to special section: regional climate modelling revisited. J Geophys Res Atm (1984–2012) 104(D6):6335–6352

Giorgi F, Mearns LO (1991) Approaches to the simulation of regional climate change: a review. Rev Geophys 29:191–216

Giorgi F, Marinucci MR, Bates GT (1993a) Development of a second generation regional climate model (RegCM2). Part I: boundary layer and radiative transfer processes. Mon Wea Rev 121:2794–2813

Giorgi F, Marinucci MR, Bates GT, De Canio G (1993b) Development of a second generation regional climate model (RegCM2). Part II: convective processes and assimilation of lateral boundary conditions. Mon Wea Rev 121:2814–2832

Grabemann I, Weisse R (2008) Climate change impact on extreme wave conditions in the North Sea: an ensemble study. Ocean Dynam 58: 199–212

Grell G (1993) Prognostic evaluation of assumptions used by cumulus parameterizations. Mon Weather Rev 121:764–787

Gualdi S et al (2013) The CIRCE simulations: regional climate change projections with realistic representation of the Mediterranean Sea. B Am Meteorol Soc 94(1):65–81

Gudmundsson L, Bremnes JB, Haugen JE, Engen Skaugen T (2012) Downscaling RCM precipitation to the station scale using quantile mapping—a comparison of methods (technical note). Hydrol Earth Syst Sci Discuss 9:6185–6201

Haerter JO, Hagemann S, Moseley C, Piani C (2011) Climate model bias correction and the role of timescales. Hydrol Earth Syst Sci 15: 1065–1079

Holthuijsen LH (2007) Waves in oceanic and coastal waters. Cambridge University Press.

Holtslag A, de Bruiin E, Pan H-L (1990) A high resolution air mass transformation model for short-range weather forecasting. Mon Weather Rev 118:1561–1575

Hosking JRM, Wallis JR (1997) Regional frequency analysis: an approach based on L-moments. Cambridge University Press

Hurvich CM, Tsai C (1989) Regression and time series model selection in small samples. Biometrika 76:297–307

IPCC (2001) Climate change 2001: the scientific basis. Contribution of Working Group I to the Third Assessment Report of the Intergovernmental Panel on Climate change, Houghton JT et al (eds), Cambridge University Press, New York, USA

IPCC (2007) Climate change 2007: the scientific basis. Contribution of Working Group I to the Fourth Assessment Report of the Intergovernmental Panel on Climate change, Solomon S et al (eds), Cambridge University Press, New York, USA

IPCC (2012) Managing the risks of extreme events and disasters to advance climate change adaptation. A Special Report of Working Groups I and II of the Intergovernmental Panel on Climate change, Field CB et al (eds), Cambridge University Press, Cambridge, UK and New York, NY, USA

IPCC (2013) Climate change 2013: the physical science basis. Contribution of Working Group I to the Fifth Assessment Report of the Intergovern- mental Panel on Climate Change Stocker TF, Qin D, Plattner G-K, Tignor M, Allen SK, Boschung J, Nauels A, Xia Y, Bex V, Midgley PM (eds), Cambridge University Press, Cambridge, United Kingdom and New York, NY, USA

Jaffe B, Sallenger A (1992) The contribution of suspension events to sediment transport in the surf zone. *Proc 23rd Inter Coast Eng Conf*, Am Soc Civ Eng, 2680–2693

Jordà G, Gomis D, Álvarez-Fanjul E, Somot S (2012) Atmospheric contribution to Mediterranean and nearby Atlantic Sea level variability under different climate change scenarios. Glob Planet Change 80–81(0):198–214

Kallos G, Nickovic S, Papadopoulos A, Jovic D, Kakaliagou O, Misirlis N, Boukas L, Mimikou N, Sakellaridis G, Papageorgiou J, Anadranistakis E, Manousakis M (1997) The regional weather forecasting system SKIRON: an overview. *Proc Interntnl Symposium on Regional Weather Prediction on Parallel Computer Environments*, 15–17 October 1997, Athens, Greece, 109–122.

Komen GJ et al (1994) Dynamics and modelling of ocean waves. Cambridge University Press, Cambridge

Krestenitis YN, Androulidakis YS, Kontos YN, Georgakopoulos G (2011) Coastal inundation in the north-eastern Mediterranean coastal zone due to storm surge events. J Coast Conserv 15(3):353–368

Lionello P, Cogo S, Galati MB, Sanna A (2008) The Mediterranean surface wave climate inferred from future scenario simulations. Glob Planet Change 63:152–162

Lionello P et al (2012) Introduction: Mediterranean climate-background information. In: *The Climate of the Mediterranean Region*. Elsevier

Maheras P, Flocas H, Patrikas I, Anagnostopoulou C (2001) A 40-year objective climatology of surface cyclones in the Mediterranean region: spatial and temporal distribution. Int J Climatol 21:109–130

Makris CV, Androulidakis YS, Krestenitis YN, Kombiadou KD, Baltikas VN (2015) Numerical modelling of storm surges in the

Mediterranean Sea under climate change. *Proc 36th International Association of Hydraulic Research (IAHR) World Congress* 28 June – 3 July, The Hague, The Netherlands

Marcos M, Tsimplis MN (2008) Comparison of results of AOGCMs in the Mediterranean Sea during the 21st century. J Geophys Res 113(C12)

Marcos M, Tsimplis MN, Shaw AG (2009) Sea level extremes in southern Europe. *J Geophys Res Oceans (1978–2012)* 114(C1)

Marcos M, Jordà G, Gomis D, Pérez B (2011) Changes in storm surges in southern Europe from a regional model under climate change scenarios. Glob Planet Change 77(3–4):116–128

Mclnnes KL, Erwin TA, Bethols JM (2011) Global climate model projected changes in 10 m wind speed and direction due to anthropogenic climate change. Atmos Sci Lettt 12:325–333

Menéndez M, Méndez FJ, Izaguirre C, Luceño A, Losada IJ (2009) The influence of seasonality on estimating return values of significant wave height. Coast Eng 56:211–219

Pal JS, Giorgi F, Bi X, Elguindi N, Solmon F, Rauscher SA, Gao X, Francisco R, Zakey A, Winter J, Ashfaq M, Syed FS, Sloan LC, Bell JL, Diffenbaugh NS, Karmacharya J, Konaré A, Martinez D, da Rocha RP, Steiner AL (2007) Regional climate modelling for the developing world: the ICTP RegCM3 and RegCNET. Bull Amer Meteor Soc 88:1395–1409

Papadopoulos A, Katsafados P, Kallos G (2002) Regional weather forecasting for marine application. Glob Atm Ocean Syst 8(2–3):219–237

Pawlowicz R, Beardsley B, Lentz S (2002) Classical tidal harmonic analysis including error estimates in MATLAB using T TIDE. Comput Geosci 28:929–937

Ris RC, Holthuijsen LH, Booij N (1999) A third-generation wave model for coastal regions: 2. Verification. J Geophys Res 104(C4):7667–7681

Roeckner E, et al. (2003) The atmospheric general circulation model ECHAM5, Report No. 349. Max Planck Institute for Meteorology, Hamburg, Germany. ISSN: 0937–1060

Rogers WE, Hwang PA, Wang DW (2003) Investigation of wave growth and decay in the SWAN model: three regional-scale applications. J Phys Oceanogr 33(2):366–389

Santos JA, Corte-Real J, Ulbrich U, Palutikof J (2007) European winter precipitation extremes and large-scale circulation: a coupled model and its scenarios. Theor Appl Climatol 87:85–102

Savvidis YG, Dodou MG, Krestenitis YN, Koutitas CG (2004) Modeling of the upwelling hydrodynamics in the Aegean Sea. Mediterr Mar Sci 5:5–18

Schoetter R, Hoffimman P, Rechid D, Schlunzen KH (2012) Evaluation and bias correction of reginal climate model results using model evaluation measures. J Appl Meteor Climatol 51:1670–1684

Slangen ABA, Adloff F, Jevrejeva S, Leclercq PW, Marzeion B, Wada Y, Winkelmann R (2016) A review of recent updates of sea-level projections at global and regional scales. Surv Geophys. doi:10.1007/s10712-016-9374-2

Smith SD, Banke EG (1975) Variation of the sea surface drag coefficient with wind speed. Q J R Meteorol Soc 101(429):665–673

Soomere T, Weisse R, Behrens A (2012) Wave climate in the Arkona Basin, the Baltic Sea. Ocean Sci 8:287–300

Soukissian TH (2005) The wave climate of the Aegean Sea: wind waves. In: *State of the Hellenic Marine Environment*, Papathanassiou E, Zenetos A (eds), Hellenic Centre for Marine Research, pp 65–73

Soukissian T et al (2008) A new wind and wave atlas of the Hellenic Seas. *Proc 27th Int Conf Offshore Mech Arctic Eng,* pp 791–799

SWAN (2012) SWAN scientific and technical documentation (SWAN Cycle III, version 40.91) http://swanmodel.sourceforge.net/online_doc/swanuse/swanuse.html

Šepić J, Vilibić I, Jordà G, Marcos M (2012) Mediterranean Sea level forced by atmospheric pressure and wind: variability of the present climate and future projections for several period bands. Glob Planet Change 86:20–30

The BACC Author Team (2008) Assessment of climate change for the Baltic Sea basin, Regional Climate Studies Series. Springer–Verlag, Berlin–Heidelberg, p. 474

Themeßl MJ, Gobiet A, Heinrich G (2012) Empirical statistical downscaling and error correction of regional climate models and its impact on the climate change signal. Clim Chang 112:449–468

Tolika K, Anagnostopoulou C, Velikou K, Vagenas C (2015) A comparison of the updated very high resolution model RegCM3_10km with the previous version RegCM3_25km over the complex terrain of Greece: present and future projections. Theor Appl Climatol . doi:10.1007/s00704-015-1583-y1–12

Trigo IF, Davies TD, Bigg GR (1999) Objective climatology of cyclones in the Mediterranean region. J Clim 12:1685–1696

Tsimplis MN, Blackman D (1997) Extreme sea-level distribution and return periods in the Aegean and Ionian Seas. Estuar Coast Shelf S 44(1):79–89

Tsimplis MN, Vlahakis GN (1994) Meteorological forcing and sea level variability in the Aegean Sea. J Geophys Res Oceans 99(C5):9879–9890

Tsimplis MN, Marcos M, Somot S (2008) Twenty-first century Mediterranean Sea level rise: steric and atmospheric pressure contributions from a regional model. Glob Planetnn 63(2): 105–111

Tsimplis MN, Calafat FM, Marcos M, Jordà G, Gomis D, Fenoglio-Marc L, Struglia MV, Josey SA, Chambers DP (2013) The effect of the NAO on sea level and on mass changes in the Mediterranean Sea. J Geophys Res (Oceans) 118:944–952

Vagenas C, Anagnostopoulou C, Tolika K (2014) Climatic study of the surface wind field and extreme winds over the Greek seas. *Proc 12th International Conference on Meteorology, Climatology and Atmospheric Physics (COMECAP)*

Van den Eynde D, De Sutter R, Haerens P (2012) Evolution of marine storminess in the Belgian part of the North Sea. Nat Hazards Earth Syst Sci 12:305–312

Van der Westhuysen AJ, Zijlema M, Battjes JA (2007) Nonlinear saturation-based whitecapping dissipation in SWAN for deep and shallow water. Coast Eng 54(2):151–170

Wang XH (2002) Tide-induced sediment resuspension and the bottom boundary layer in an idealized estuary. J Phys Oceanogr 32:3113–3131

Wang S, McGrath R, Hanafin JA, Lynch P, Semmler T, Nolan P (2008) The impact of climate change on storm surges over Irish waters. Ocean Model 25:83–94

Young IR (1999) *Wind Generated Ocean Waves*. Elsevier Ocean Engineering Series

Zecchetto S, De Biasio F (2007) Sea surface winds over the Mediterranean Basin from satellite data (2000–04): meso- and local-scale features on annual and seasonal time scales. J Appl Meteorol Climatol 46(6):814–827

Zervakis V, Georgopoulos D, Drakopoulos PG (2000) The role of the North Aegean in triggering the recent eastern Mediterranean climatic changes. J Geophys Res 105(C11):26103–26116